A large mid-infrared spectroscopic and near-IR imaging survey of ULIRGs: their nature and evolution [1] [2]

D. Rigopoulou[1], H.W.W. Spoon[1,2], R. Genzel[1], D. Lutz[1], A.F.M. Moorwood[2], Q.D. Tran[1]

Received _____; accepted _____

To appear in the Astronomical Journal

[1]Based on observations with ISO, an ESA project with instruments funded by ESA member states (especially the PI countries: France, Germany, the Netherlands, and the United Kingdom) with the participation of ISAS and NASA.

[2]Based on observation collected at the European Southern Observatory, Chile, ESO No 62.P-0315.

[1]Max-Planck-Institut für extraterrestrische Physik, Postbox 1603, D-85740, Garching, Germany

[2]European Southern Observatory, Karl-Schwarzschild-Strasse 2, 85748 Garching, Germany

ABSTRACT

We present a low resolution mid-infrared spectroscopic survey of an unbiased sample of 62 Ultraluminous Infrared Galaxies (ULIRGs) ($L_{IR} > 10^{12}$ $L_{\odot}$, z$\leq$0.3) using ISOPHOT-S on board the Infrared Space Observatory (ISO). For comparison we also present ISOPHOT-S spectra for 23 active galactic nuclei (AGN) and 15 starburst and normal galaxies. The line-to-continuum ratio of the 7.7 μm PAH emission feature is used as a discriminator between starburst and AGN activity in ULIRGs. We find that the majority of ULIRGs are predominantly powered by starbursts. The ratio of PAH over infrared luminosities, L_{PAH}/ L_{IR}, for starburst dominated ULIRGs is very similar to the ratio found for template starbursts. The shapes of the PAH features are sometimes unusual. Extinction has a noticeable effect on the PAH spectra of ULIRG starbursts.

We have obtained high resolution near-infrared imaging for the Southern ISOPHOT-S ULIRGs to investigate their evolution stage. The majority (68%) of the ULIRGs imaged are double systems and all show distorted morphologies. From the 23 double nuclei systems 17 of them appear at linear separations between 4-14 kpc with a mean separation of 6.5 kpc. Using the separations measured from our new near-infrared imaging as well as from the literature, we have examined whether ULIRGs that are advanced mergers are more AGN-like. We have found no such evidence contrary to what is postulated by the classical evolutionary scenario. No correlation is found between the stage of merger in ULIRGs and their infrared luminosity. In fact we find that systems in the early stages of merging may well output maximum luminosity. We also find that the total mass of interstellar gas, as estimated from the CO (1$\rightarrow$0) luminosity, does not decrease with decreasing merger separation. When both an AGN

and a starburst occur concurrently in ULIRGs, we find that the starburst dominates the luminosity output. We propose that the available gas reservoir and the individual structure of the interacting galaxies plays a major role in the evolution of the system.

Subject headings: galaxies: active – galaxies: starburst – infrared: galaxies

1. Introduction

With bolometric luminosities and space densities comparable to those of quasars (Soifer et al. 1987), ULIRGs are the dominant population of luminous galaxies in the local Universe. Sanders and Mirabel (1996) have reviewed the properties of ULIRGs which can be summarized as follows: (1) most of the bolometric luminosity of ULIRGs is emitted at far-infrared (12-100 μm) wavelengths, (2) all ULIRGs are invariably very dust and gas rich systems (e.g. Rigopoulou et al. 1996a, Solomon et al. 1998), (3) most ULIRGs are interacting systems (e.g. Leech et al. 1994) with distorted morphologies. The quasar like luminosities of ULIRGs led Sanders et al. (1988) to propose an evolutionary scenario where most ULIRGs are predominantly powered by dust enshrouded quasars.

For almost a decade, one subject of debate has been centered on the issue of whether the dominant luminosity source of ULIRGs is an AGN or a starburst. The ULIRG spectrum from the radio to infrared displays characteristics similar to those of starbursts (Condon et al. 1991, Crawford et al. 1996, Rowan-Robinson and Crawford 1989, Rigopoulou et al. 1996b, etc), and the powerful "starburst winds" detected in some of them (Armus et al. 1990, Heckman et al. 1990) are usually associated with starbursts. However, optical spectra resembling those of Seyfert galaxies (Sanders et al. 1988, Kim et al. 1995), and hard X-rays, a signpost of AGN activity (Ogasaka et al. 1997, Kii et al. 1997), have been detected in some ULIRGs. In reality, probably both starburst and AGN occur simultaneously in ULIRGs.

Along with the plethora of observational data on ULIRGs, it has become all the more evident that interactions and mergers are at the heart of the ULIRG phenomenon. Dynamical modeling has demonstrated that galaxy interactions and mergers are efficient means of driving central inflows of gas (Noguchi et al. 1991, Barnes and Hernquist 1996, Mihos and Hernquist 1996).

Optical imaging (Leech et al. 1994, Clements et al. 1996) has shown that virtually all ULIRGs are interacting however, dust obscuration has not allowed a full investigation of the interactions since some of the nuclei are deeply embedded. That dust really plagues the appearance of ULIRGs in the optical has also been demonstrated through recent WFPC2 imaging (Borne et al. 1998). In order to study the interaction and merging process in ULIRGs high resolution imaging at longer wavelengths, such as the near-infrared (NIR) regime, is necessary. With the advances in detector technology high resolution imaging in the NIR is now possible allowing one to penetrate through the obscuring dust. So far, high resolution NIR imaging has been carried out for few individual objects (Carico et al. 1990, Majewski et al. 1993, Armus et al. 1995) while Murphy et al. (1996) and Duc Mirabel and Maza (1997) presented NIR images for somewhat larger samples but with resolution inadequate to study in detail the various morphological features.

With the advent of the Infrared Space Observatory (ISO) of the European Space Agency (Kessler et al. 1996) mid-infrared spectroscopy became available for a large sample of ULIRGs (Genzel et al. 1998), enabling reconsideration of the energetics and the evolution of ULIRGs. Observations of mid-infrared fine structure lines with the Short Wavelength Spectrometer (SWS) as well as of polycyclic aromatic hydrocarbon (PAH) features found in emission at 6.2, 7.7, 8.6 and 11.3 μm with the ISOPHOT-S for a sample of 15 ULIRGs (Genzel et al. 1998), show that these are powerful tools in probing the luminosity source in ULIRGs. Ground based observations of PAH features in a variety of environments have shown that PAH are in principle strong in starburst galaxies but weak or absent in classical AGN (Moorwood 1986, Roche et al. 1991). The observations of Genzel et al. (1998) showed that on average ULIRGs are starburst powered. To put these initial results in a more secure statistical footing the observations were expanded to yet a larger sample of 62 ULIRGs observed with the ISOPHOT-S, focusing on the spectral regime from 5 to 11 μm, where most of the PAH features arise. First results from this survey have been summarized in

Lutz et al. (1998) where it was shown that 80% of ULIRGs display starburst characteristics with only a 20% showing signs of AGN activity.

In this paper we present the full atlas of ISOPHOT-S spectra for 62 ULIRGs. As discussed in Genzel et al. (1998) and Lutz et al. (1998) the PAH feature line-to-continuum is a robust tool to discriminate between starburst and AGN activity in ULIRGs. For comparison we present ISOPHOT-S spectra for template AGN and starbursts. In addition, to gain more insight into the peculiar morphology of the ISOPHOT-S ULIRGs we have obtained high resolution NIR images for a subsample of Southern ULIRGs. We combine the ISO results with our high resolution imaging and probe the evolution of ULIRGs. The structure of the paper is as follows: the ISOPHOT-S sample is presented in section (2) followed by the Observations and Data Reduction section (3) for both the ISO measurements and the NIR imaging. In Section 4 we present our results from the ISOPHOT-S spectroscopic survey for ULIRGs, AGN and starbursts. In section (5) the morphology of ULIRGs is presented together with a discussion on the importance of tails as evolution indicators. A simple observational test of the evolution of ULIRGs together with a discussion on merging modeling is presented in section (6) while in section (7) we discuss possible evolutionary scenarios.

2. ULIRG Sample

The ISOPHOT-S sample (hereafter ISO-ULIRG sample) has been drawn from the complete IRAS 2 Jy (Strauss et al. 1992) and its extension IRAS 1.2 Jy sample (Fisher et al. 1995). The selection of ULIRGs was based on the following criteria:

- luminosity $L_{FIR}(40-120) > 10^{11.7}$ $L_\odot$ (which corresponds to $L_{IR}(8-1000) \sim 10^{12}$ $L_\odot$)[5]
- flux S_{60} >1.3 Jy
- good ISO visibility
- redshift below 0.3. The constraint on redshift was imposed to ensure that the 7.7 μm PAH feature did not shift into regions of poor sensitivity in the ISOPHOT-S detector.

No color criteria have been applied to the sample so as to not bias it towards AGN. The sample includes some of the bright BGS ULIRGs (Sanders et al. 1988) that meet our selection criteria. In addition we have included IRAS 23060+0505 ($S_{60} \sim 1$ Jy) and NGC 6240 (less luminous however, it exhibits ULIRG characteristics). Accurate positions for the ISO-ULIRG sample were taken from VLA observations (Crawford et al., 1996), optical images (Clements et al. 1996), or from the Automated Plate Measuring Machine (APM) using a likelihood technique. Objects with inaccurate positions have been dropped from our ISO sample as well as objects with poor ISO visibility. A few objects were not observed due to the end of the ISO mission. All these effects do not pose any bias in our sample. Preliminary results of the ISOPHOT-S sample have been presented in Genzel et al. (1998), (for most of the BGS members) and Lutz et al. (1998). Throughout the paper we have used $H_0 = 75$ km s^{-1} Mpc $^{-1}$ and $q_0 = 0.5$.

In addition to the ISO-ULIRG sample described above, 4-16 μm spectra have been obtained with ISOCAM (as part of the ZZULIRG project) for a further 16 ULIRGs (hereafter ISO-ZZULIRG). This sample specifically populates the higher luminosity bins

[5]See e.g. Sanders & Mirabel (1996) for the definition of the 40-120 μm L_{FIR} and 8-1000 μm L_{IR} luminosities

($L > 10^{12.25}$ $L_\odot$). A detailed analysis of the ZZULIRG sample will be presented elsewhere (Tran et al. 1999).

Imaging data were collected for 27 out of the 43 ISO-ULIRG plus ISO-ZZULIRG galaxies with declinations $\delta \leq 3^o$ accessible to telescopes in the Southern Hemisphere. We have not imaged ISO-ULIRGs for which previous high quality imaging data existed. Also we avoided those ISO-ULIRGs with already available NICMOS data.

3. Observations and Data Reduction

3.1. PHOT-S observations

We obtained low resolution ($\lambda/\Delta\lambda \sim$90) 2.5–11.6 μm spectra for the entire ISO-ULIRG sample using the ISOPHOT-S spectrophotometer (Lemke et al. 1996) onboard ISO (Kessler et al. 1996). In addition to the ULIRG spectra we have obtained ISOPHOT-S spectra for 23 AGN and 14 starburst and normal galaxies to be used as comparison templates. ISOPHOT-S comprises two low-resolution grating spectrometers covering simultaneously the wavelength range 2.47 to 4.87μm and 5.84 to 11.62μm. The spectrum is registered by two linear arrays of 64 Si:Ga detectors with a common entrance aperture of $24'' \times 24''$. For the observations described here we only make use of the long-wavelength section, because the signal-to-noise ratio (S/N) for all but the brightest members of the ISO-ULIRG sample is very low in the short-wavelength regime. The measurements were carried out in rectangular chopped mode, using a chopper throw of $180''$. The resulting spectra are thus free of contributions from zodiacal light, that would otherwise seriously affect the faint ULIRG spectra. The pure on-source integration times vary between 512 and 2048 s for ULIRGs and 128 – 2048 s for AGN and starbursts.

The ISOPHOT-S data were reduced using PIA version 7.2.[6] The data reduction steps can be summarized as follows:

1) deglitching on ramp level

2) subdivision of ramps in sections of 32 non destructive read-outs (NDRs), which greatly increases the effectiveness of statistical tools (to be carried out in step 4) and takes care of minor ramp non-linearity effects. For faint targets such as the ULIRGs, the gain in statistics prevails

3) ramp fitting to derive signals

4) masking of bad signals by eye-inspection

5) kappa sigma and min/max clipping on remaining signal distribution

6) determination of average signal per chopper plateau

7) masking or correction of bad plateaus by eye-inspection

8) background subtraction using all but the first two plateaus, and finally,

9) flux calibration, using the default PIA version 7.2 spectral response function (SRF).

Since ISOPHOT-S was operating close to its sensitivity limits, the detector response to changes of illumination consists of an immediate jump to an intermediate level, followed by an extremely slow transient to the final signal level. In practice, only the initial step is observed. To correct for this effect, we applied a flux correction factor of 1.4 (U. Klaas 1997, private communication) to all our chopped ISOPHOT-S spectra.

We have compared the PIA version 7.2 default SRF with the signal dependent SRF of Acosta-Pulido (1999) for the case of faint ULIRGs. The comparison showed that the overall flux correction factor (1.4) we applied to our spectra calibrated with the default SRF brings these results close to those obtained by using the signal dependent SRF without correction

[6]PIA is a joint development by the ESA Astrophysics Division and the ISOPHOT Consortium.

factor. Only towards the longest PHT-SL wavelength pixels does our overall correction factor tend to be too large. For the PHT-SS range the situation is quite different. Here the signal dependent SRF not only drastically changes the continuum slope, it also removes the deep 3.1μm pseudo-"ice" feature present in most of our standard calibrated AGN and starburst comparison spectra. Since this feature always appears at the same *observed* instead of *rest* wavelength it follows that the feature cannot be real. We conclude that the calibration for the useful part of our ISOPHOT-S spectra (the 5.8–11μm range) is good, and moreover, internally consistent.

3.2. Near-Infrared Imaging

We have obtained high quality NIR images for 27 out of the 43 ISO galaxies with declinations $\delta \leq 3^o$ accessible to telescopes in the southern hemisphere. Near-infrared imaging for the 27 southern ISO-ULIRG plus ISO-ZZULIRG galaxies was carried out in November 1998 with the SOFI (Moorwood, Cuby and Lidman 1998) near-infrared imaging camera, installed on the ESO-NTT telescope, LaSilla. For the observations we used the J band and K_s band filters with central wavelengths 1.247 μm and 2.162 μm, respectively. The SOFI detector is a Hawaii HgCdTe 1024×1024 array. For the current observations the projected scale of the array is $0''.144$ pixel^{-1}. Sky conditions were photometric throughout the acquisition of the images. For each galaxy observations of a nearby star were made in order to obtain an accurate estimate of the point spread function (PSF) at the time of the observation. Integration time per frame was set to 20 sec, reaching a total integration time of 20 mins for the K_s band (except for 01355-1814 for which integration time in K_s was 8 mins) and 6 mins for the J band.

The observations were carried out using the "jitter" technique which is the most efficient method of sky acquisition with a minimum loss of observing time. In this technique

the telescope is offset around the central position (the offsets were generated randomly but were restricted within a 20″ square box around the central position) by small amounts. A typical acquisition in jitter mode consisted of 6 frames for the J- band and 20 frames for the K_s band. Sky estimation and subtraction, flat-fielding (based on dome-flats), plane-recentering, and frame-coaddition were all performed using the "jitter" algorithm which is part of the ECLIPSE software collection designed especially for the reduction of SOFI and ISAAC images (Devillard 1997).

The photometry has been carried out in IRAF using circular apertures centered on each nucleus. For flux calibration , faint stars from the NICMOS, UKIRT Faint Standards lists have been observed before and after the galaxy observations. Under the excellent seeing conditions (FWHM range between 0.45″ – 0.8″) we estimated that the errors in the reported magnitudes are less than 0.08 mag. Figure 1 presents the calibrated K_s contour maps of the 27 galaxies that we have observed (since for the current discussion we only use the K_s band data we only present those maps. The J band data will be discussed in a forthcoming paper). The linear scale is indicated.

4. ISOPHOT-S Results

4.1. PAH features

The 3-12 μm window in the spectra of most galaxies contains a number of broad emission features, the most important being at 3.3, 6.2, 7.7, 8.7 and 11.2 μm. These features appear whenever the interstellar medium is exposed to moderately intense UV radiation (see e.g. review in Puget & Léger 1989). The carriers of these features are either large carbon-rich molecules, the so-called Polycyclic Aromatic Hydrocarbons (PAH), or very small grains consisting of amorphous aromatic carbons (e.g. Sakata et al. 1987). Although

the precise nature of the carriers is still somewhat uncertain, we will refer to them as "PAH" which is one of the most popular identifications, noting that their use as a diagnostic tool for external galaxies is unaffected by this uncertainty. Since their first discovery as "unidentified" features (Gillett et al. 1973), the mid-infrared features have been detected in a variety of Galactic environments. ISO observations are adding substantial detail to PAH feature studies of galactic regions relevant to extragalactic studies, such as PDRs, HII regions (e.g. Verstraete et al. 1996, Roelfsema et al. 1996), and the diffuse emission of the galactic disk (Mattila et al. 1996).

Prior to ISO, studies of PAH features in galaxies were limited. Following their discovery in the spectrum of M82 (Gillett et al. 1975, Willner et al. 1977), several studies noted that starbursts exhibit more prominent PAH features than Seyferts, in the latter the emission is usually either weak or absent (e.g. Moorwood 1986, Roche et al. 1991). With ISO we can now study the PAH emission in a large, unbiased sample of ultraluminous galaxies, which we have supplemented by starburst and AGN comparison objects.

4.2. ISOPHOT-S Spectroscopy

The spectra for the 62 ULIRGs, the template AGN and starbursts observed with ISOPHOT-S are shown in Figures 2, 3 and 4 respectively. Among the AGN templates there are several known composite sources with both AGN and starburst activity. For instance, NGC 7469 is a Seyfert 1 nucleus surrounded by a star forming ring which contributes up to two thirds of the bolometric luminosity (Genzel et al. 1995). A starburst ring is also contributing to the bolometric luminosity of Circinus (Moorwood et al. 1996), the radio galaxy Cen A, and the narrow line X-ray galaxy NGC 7582. Our ISOPHOT-S data for the template AGN and starbursts confirm the findings from previous observations (e.g. Roche et al. 1991): we find that the 7.7 μm emission feature is strong in dusty environments with

moderately strong UV radiation fields, such as those found in starbursts. PAH emission becomes significantly weaker in very strong radiation fields such as those found in AGN. Overall, the strength of the PAH line to continuum ratio in AGN is about an order of magnitude weaker than the template starbursts. The strength of the 7.7μm emission feature in the above mentioned composite galaxies ranges between these two extremes.

The majority of the ULIRG ISOPHOT-S spectra show PAH features at 6.2, 7.7 and 8.6 μm similar to those seen in starburst galaxies. This is also evident in their average spectrum, presented in Figure 1 of Lutz et al. (1998). Given that ULIRGs may host starburst and AGN, we assume the PHT-S spectra to be a superposition of a PAH dominated starburst spectrum and a continuum dominated AGN spectrum, both likely modified by significant obscuration. To estimate the relative contributions, we use here a simple empirical method also employed by Genzel et al. (1998) and Lutz et al. (1998), based on the line-to-continuum ratio of the strongest feature (7.7μm). We show in Figure 2 the continua we have adopted in this process.

Continuum determination is important and not trivial, since the 5-11 μm range is characterized by a multitude of features. The PAH emission features overlap with each other and with the broad silicate absorption centered at 9.6 μm, and this overlap is likely to be important for obscured galaxies like ULIRGs. We have determined the continuum by linear interpolation between two pivot points at 5.9 μm and 10.9 μm (both rest wavelength). For objects whose redshift moves the 10.9 μm point out of the observed range we used the empirical formula $S_{10.9} = (2.5 \pm 0.5) \times S_{5.9}$ which we found adequate for low redshift sources. Continuum determination by eye was done for a handful of template AGN where the method described above gave unphysical results (for instance interpolated 7 μm continuum above the observed spectrum). The peak strength of the 7.7μm feature was measured by simply taking the average of all data within a window covering the

rest wavelengths 7.57–7.94 μm. Finally, the ratio of feature minus (local) continuum and continuum was determined. Errors or limits on all these quantities are based on the noise measured shortward of 5.9 μm rest wavelength and the increase in noise towards longer wavelengths corresponding to the decrease of the ISOPHOT-S spectral response.

The selected 5.9 μm point is largely free of feature emission and provides a secure point for the continuum determination. On the other hand, the 10.9 μm point is less securely determined since it is still within the long wavelength side of the silicate absorption feature. Therefore, one can assume that our adopted continuum is a "lever" which can be rotated significantly around the 5.9 μm point. The placement of the 10.9 μm continuum level is not arbitrary and the slope of the continuum cannot be very steep. There is a physical reason for this: the 10.9 μm point should be such that the resulting continuum should never rise above the data in the 6.5–7.7 μm range since the PAH features are known to sit on a plateau of the same origin. Although the uncertainty in placement of the continuum can affect the strength of the 7.7 μm PAH L/C, it will not turn a "strong PAH" into a "weak or absent PAH" and therefore our method in separating starbursts from AGN based on PAH features remains robust.

Low resolution spectra of the 6.2–11.3 μm PAH features and the underlying plateau are usually well fit by Lorentzian or Cauchy functions (e.g. Boulanger et al. 1998 for PDRs, Mattila et al. 1999 for the galaxy NGC 891). For the ULIRGs we do not adopt such a fitting procedure to keep our method unbiased towards a "canonical" PAH shape which will not be adequate for low feature-to-continuum ratio systems like Mrk 231 whose weak feature, be it of PAH or different origin, is not fit well by a standard PAH shape. Similar results to those presented in this work are obtained using two other methods to quantify the relative importance of PAH emission (Tran et al. 1999). In the first one, the importance of PAH features is determined from a simple ratio of fluxes measured in two narrow bands

at 7.7 and 5.9 μm. The other method implements a more elaborate fit of the data, using variable contributions of an AGN continuum and a starburst PAH spectrum, both affected by (different) extinction.

The feature-to-continuum ratio of the 7.7μm PAH feature is presented in Tables 1, 2 and 3 for the ISOPHOT-S ULIRG sample, the AGN and the starburst templates, respectively. Along with other information we quote the flux densities at 5.9 and 10.9μm, the points used for continuum determination. Table 4 gives values for the properties of the *averaged* ULIRG, starburst and AGN spectrum (see Lutz et al. 1998). The strength of the 7.7 PAH L/C is used to classify ULIRGs as starbursts or AGN. All ULIRGs with a 7.7 PAH L/C $\leq$1 (or upper limits slightly above 1) are classified as AGN and the rest as starbursts.

4.3. L_{PAH}/L_{IR}: are starburst dominated ULIRGs similar to starbursts ?

In Figure 5 we compare the properties of ULIRG-starbursts (those ULIRGs with PAH L/C $>$ 1) to those of the template starbursts (all starbursts from Table 3 except M81, M51 and NGC 4569). In each case we compute the ratio of the 7.7μm PAH luminosity, L_{PAH}, over far-infrared L_{IR} luminosities. As can be seen from Figure 5 the distribution of the L_{PAH}/ L_{IR} is found to be similar in ULIRG-starburst and template starbursts. The mean L_{PAH}/ L_{IR} value for starbursts is 8.13×10^{-3}, only 1.4 times larger than the value found for ULIRG-starbursts. The L_{PAH}/ L_{IR} ratio provides an estimate of the "activity" of the galaxy in the sense that the more starbursting activity a galaxy shows the smaller the ratio becomes due to the higher infrared luminosity (e.g. Acosta-Pulido et al. 1996).

Mattila et al. (1999) show that the 5.9–11.3 μm PAH luminosity in NGC 891, a normal non-starburst system, makes up 9% of the total IR luminosity of the system. Allowing for the difference between 7.7 μm luminosity and "total" PAH emission (5.9–11.3 μm) we

find that in a normal galaxy the PAH emission contributes a higher fraction to the total IR radiation than in a starburst galaxy. Moving the comparison to ULIRG-starbursts and starbursts we see exactly the same trend: ULIRG-starbursts show a somewhat lower L_{PAH}/L_{IR} ratio (log[mean value] = -2.26) than the template starbursts (log[mean value] = -2.09). Nonetheless, the comparison of the L_{PAH}/L_{IR} ratios implies that ULIRG-starbursts have similar properties to template starbursts and that our method to separate ULIRG-starbursts from ULIRG-AGN is correct.

4.4. The effect of extinction on ULIRG PAH spectra

A close inspection of Figure 2 suggests that the observed ratios of the PAH features in ULIRGs differ somewhat from those in lower luminosity starbursts which exhibit rather homogeneous PAH properties. For only a few individual ULIRGs like Arp 220 is the S/N of the ISOPHOT-S spectra sufficient to show this effect, but the average ULIRG spectrum (Lutz et al. 1998) confirms its overall relevance. Compared to the 7.7 μm feature, which is the strongest feature in ULIRGs as well as in starbursts, the 6.2 μm and 11.3 μm (where available) features are somewhat weaker in the ULIRGs. The same applies to the 8.6 μm feature which is sometimes just a shoulder of the 7.7 μm feature rather than a well-separated feature (see e.g. the case of Arp 220).

The weakness of 6.2 and the 8.6 μm features may reflect intrinsic variations related to the unusual conditions in the interstellar medium in ULIRGs. There is evidence for such variations from ISO observations of HII regions and reflection nebulae in our own Galaxy (e.g. Verstraete et al. 1996, Roelfsema et al. 1996, 1998, Cesarsky et al. 1996). Various explanations including changes in the PAH species mix, PAH dehydrogenization, and PAH ionization have been put forward by these authors. Some of the H II region spectra of Roelfsema et al. (1998) resemble the average ULIRG spectrum, due to intrinsic

variations or due to extinction, as suggested below for the ULIRGs. While most PAH spectra of our comparison starbursts (Fig. 4) are remarkably similar, we believe that a real intrinsic variation is present in at least one source, the low metallicity starburst NGC 5253. Similarly, the faint residual (PAH?) features in the spectrum of NGC 1068 do not fit a normal PAH spectrum.

We believe, however, that the dominant influence on the ULIRG PAH ratios is extinction. This has already been suggested by Lutz et al. (1998) on the basis of an overall consistency between average ULIRG extinction derived from SWS spectroscopy, (extinction-induced) weakening of the 6μm continuum, and PAH ratio variations. In Figure 6 we illustrate the effect of extinction by comparing the Arp 220 PHOT-S spectrum with the M82 spectrum for which additional screen extinction of $A_V \sim 20$ and $A_V \sim 50$ has been applied. The M82 spectrum is the ISO-SWS spectrum (Förster-Schreiber 1999) degraded to PHT-S resolution. In such an obscured starburst spectrum, the 11.3 μm feature is weak, the 8.6 μm feature has become a shoulder of the stronger 7.7 μm feature, and the 6.2 μm feature has been suppressed relative to the 7.7 μm one, similar to what we observe for the ULIRGs. The assumed screen extinction is, of course, a simplification, and uncertainties in the extinction curve cannot be ignored. Nevertheless, these feature changes due to obscuration reproduce well the features of Arp 220, considering that the 11.3μm feature of Arp 220 is on top of a stronger continuum. This steeply rising continuum is difficult to locate at the end of the PHOT-S spectrum, but seen more clearly in the data of Charmandaris (1997) and Smith et al. (1989). Most plausibly, it reflects the extreme concentration of star forming activity in the inner few 100 parsecs of Arp220, leading to a stronger "warm" continuum due to HII regions in terms of the three component model of Laurent et al. (2000).

The effect of extinction on the 6.2/7.7 μm PAH ratio is demonstrated in a more quantitative way in Figure 7. Here, the 6.2/7.7 PAH flux ratio is plotted as a function of

the extinction A_V as estimated from independent ISO-SWS spectroscopy (from Genzel et al. 1998, values converted to screen case)[7]. To estimate the extinction A_V we used the extinction curve of Draine (1989) together with the extinction curve derived from ISO–SWS data on the Galactic center (Lutz et al. 1996). The total 6.2μm and 7.7μm feature fluxes have been derived by simple integration of the continuum-subtracted spectrum over the rest wavelength ranges 6.0-6.5 and 7.3-8.2μm, respectively. The diagram includes data for template starburst galaxies, the molecular ring in the Galactic Center, and for those ULIRGs for which extinction estimates are available from SWS spectroscopy. Figure 7 shows that there is a clear anticorrelation between the 6.2/7.7 PAH ratio and extinction. Of the templates, NGC 4945 and the molecular ring in the Galactic Center have extinctions that approach those of ULIRGs. Interestingly, those are the only templates that show low 6.2/7.7 PAH ratios and their 8.6 μm features appear as a shoulder of the 7.7μm feature rather than as a separate feature, due to suppression in the wings of the silicate absorption feature. How robust is the 6.2/7.7 μm ratio to the location of the underlying continuum in our method of measuring feature fluxes? We have used the Arp 220 spectrum as a test case and varied the 10.9 μm continuum point between ∼70 and ∼400 mJy. Within this range the 6.2/7.7 μm feature ratio changes between 0.18 to 0.20 but stays well below the typical lower extinction starburst values (Figure 7). Thus our conclusion is robust to plausible variations in the continuum.

With extinction being important, could the observed ULIRG PHT-S spectra in fact be explained by pure absorption of a smooth underlying continuum? The ISO spectra of heavily obscured young stellar objects (e.g. d'Hendecourt et al. 1996, Whittet et al. 1996) show a "pseudo emission feature" created by a decrease in absorption between the broad

[7]We assume that the obscuration is due to a foreground screen of dust with optical depth $\tau(\lambda) = 0.916A(\lambda)$

9.6μm silicate feature and the shorter wavelength 6.8 and 6.0 μm absorption features. With limited wavelength coverage, this could be misinterpreted as PAH emission. This is likely not the case for the ULIRG PHOT-S spectra, however. Firstly, the ULIRGS have a clear 6.2 μm emission feature. In an absorption spectrum, such as the above mentioned young stellar objects, another "pseudo-emission" can arise between the 6.0 and 6.8 μm features, but its peak will be at about 6.5 μm (d'Hendecourt et al. 1996, Whittet et al. 1996), incompatible with the ULIRG observations. Secondly, the short wavelength rise of the 7.7 μm feature in the ULIRG spectra is very steep. This is typical for PAH emission, but not easily reproduced with an absorption spectrum. An ambiguity exists for the feature at 8 μm. Self-absorbed silicate emission from an AGN torus (e.g. Pier and Krolik 1992) could mimic the PAH feature here. While its role in some of the more AGN-like ULIRGs remains to be investigated, we find this explanation implausible for the ULIRGs given the steep short wavelength rise of the 7.7 μm feature in both the average ULIRG spectrum and individual starburst-like ULIRGs like Arp 220.

Since extinction is affecting the strength of the PAH features, with the 6.2, 8.8 and 11.3 μm being suppressed more than the 7.7 μm, it is rather uncertain to derive the strength of the PAH features based only on the 11.3 μm strength alone as Dudley (1999) has done, in particular if the PAHs are assumed to be unobscured. Such a PAH determination is likely to underestimate the real strengths of the features. Any attempts to model the strength of PAHs should include extinction effects.

5. ULIRGs: interacting/merging galaxies

5.1. Infrared Morphologies

That mergers and interactions play an important role in the formation and evolution of ULIRGs is now well established (e.g. Sanders and Mirabel, 1996). In this section we focus on the morphology of individual targets and aim to understand the transition through the various stages of the merging process, as might be delineated through our near-infrared imaging. Nuclear separations of all the sample galaxies with apparent double nuclei have been measured: angular and linear separations respectively are shown in columns 5 and 6 of Table 5 for our ISO-ULIRG sample, and columns 2 and 3 of Table 6 for the ULIRGs whose separations were taken from the literature or from the NICMOS archive. In order to classify a ULIRG as a double nucleus system, both nuclei must be clearly visible and spatially distinct in the K_s-band images. Almost all double nuclei are at same redshift as determined by our followup near-infrared spectroscopy (Rigopoulou et al. 1999) or published optical spectroscopy (Duc Maza and Mirabel 1997, Kim et al. 1998)

It is obvious (Figure 1) that the vast majority of the ISO-ULIRGs appear to be double, interacting, merging systems. Of the 27 objects we imaged and the additional 6 NICMOS objects, 68% appear to have double nuclei, with a wide range of projected separations between the nuclear components. Moreover, features such as tidal tails, bridges connecting nuclei, double (or even multiple) nuclear peaks stress the connection between enhanced far-infrared emission and galactic interactions (e.g. Joseph & Wright 1984, Cutri & McAlary 1985 etc). We discuss the importance of tails in section 5.2.

Only two of the single-nuclei ULIRGs, 01003–2238 and 05189–2524, appear to be star-like with no sign of recent merging activity. Most single nuclei show clear signs of interactions: 23578–5307, 00406–3127, 00183–7111 01199–2307, 20049-7210, 23529-2119, 00397-1312 all show fairly extended structure.

Among the close double/interacting nuclei, there appears to be a variety of

morphological differences. The nuclear separations as a function of the recessional velocities for the ISO-ULIRG sample as well as ULIRGs with additional literature data are plotted in Figure 8. The single nuclei are plotted with upper limits on their nuclear separations. Separations down to 1″ are detected out to large recessional velocities although these velocity bins above 80000 km/s are underpopulated in the initial ULIRG sample. However, this does not introduce any bias in the classification scheme or in the nuclear separations statistics.

Double nuclei systems vary from close nuclei like 03521+0028, 06009-7716 and 04063–3236, to more distant interacting members like 01166–0844, 04114–5117 and finally to systems where the interaction involves more than two nuclei. Representative members of the the latter category include 02411+0354 (at least three nuclei visible in the NIR) 06206-6315 and systems like 23389–6139 and 0019–7426. The closest measured projected nuclear separation is that of 23230–6926 (1.03 kpc) while the most widely separated pair is 00188–0856 (projected linear separation 14.11 kpc) which may well be a characteristic example of a still well separated system, probably in the early stages of the merging process.

The case of chance superpositions, ie the possibility that some of the double nuclei objects are simple superpositions of field galaxies, could affect the classification of the double nuclei systems. However, as Murphy et al. (1996) point out the chance that a field galaxy will overlap with a particular ULIRG is smaller than 1%. Projection effects could in principle affect the classification of ULIRGs. However, as we discuss in more details in section 6, deprojected nuclear separations are larger than the projected ones and are only affecting the relative distance between the two nuclei but not the single vs double nucleus classification.

Figure 9 shows a histogram of the separations of the various ISO-ULIRGs. We find that among the 23 ULIRGs with measured separations, 17 of them are found at separations

between 4-14 kpc with a mean separation of about 6.5 kpc. Among the 23 double nuclei systems 18 of them have measured PAH L/C (for the rest of them the S/N is too low to make an accurate determination of the continuum of the 7.7 μm feature). Out of those 18 ISO-ULIRGs, 14 of them have a PAH L/C > 1 implying starburst dominating luminosity. Among the remaining 15 single (or unresolved double) nuclei ULIRGs, 13 of them have measurable PAH L/C and among those only 6 of them have PAH L/C < 1. These simple statistical findings imply that there is no clear trend for the single nuclei ULIRGs to show more AGN-like characteristics. This issue is discussed in more detail in section 6.

5.2. Tidal Tails and Mergers

Toomre and Toomre (1972, hereafter T&T) were among the first to model the creation of tidal tails and bridges in galaxies. Further numerical simulations (e.g. Barnes and Hernquist 1996) established that tidal tails can be used to assess the stage of the interaction. Tidal tails can therefore be considered as a useful "clock of the interaction".

We use tails and bridges to probe the interaction/merger status, adopting the following classification. According to our scheme, ULIRGs can be classified as follows: (a) fully relaxed systems, where we see only a single point-like nucleus with relatively little or no tails, (b) systems where the merger is completed, in such systems we see a single nucleus but with significant residual structure or tail formation (c) interacting pairs where the interacting nuclei are clearly visible and can be found in a variety of separations. The classification of the ISO-ULIRGs according to the presence of tails is shown in Table 5. Although the classification of ULIRGs is somewhat subjective (for a proper classification dynamical evidence is also needed), our intention in the following discussion is to stress the importance of the detailed morphological structure (ie tails) in assessing the stage of the interaction. For each category we discuss a few selected examples.

How many galaxies do we find in each of the above mentioned categories? Starting from the quiescent stage, the fully relaxed systems (category a) we note that we find only two such systems, 05189-2524 and 01003-2524. In the next stage, completed mergers (category b), there is quite a diversity. There are systems like 00406-3127, 01298-0744, 23529-2119, 00397-1312 and 00183-7111 which show distorted morphologies with some tails, although not as pronounced. It is very probable that these systems have completed the merger and are now slowly evolving into a more relaxed system. In the same category (b) we have classified 23253-5415, 02455-2220 and 23578-5307, all three systems show pronounced tails implying a rather recent completion of the merging process. The giant arm coming off the S side of 23523-5415 implies that the interaction has just been completed or that the projection is not favorable (there is no sign of a second nucleus). Similarly, 02455-2220 appears to be a single nucleus object with a long tail running NE of the galaxy's main body. Finally, 23578-5307 displays similar characteristics. Again, the main (merged) galaxy shows a disturbed morphology, while an arm-like structure extends to the E, SE of the main body of the galaxy. Most probably all these systems have just completed the merger phase, however, the relics of the interaction are still prominent.

However, it is not always that single nucleus objects (ie advanced mergers) display tails. Many of the galaxies which we classified as interacting pairs, (category c) show extended structure, tails and/or bridges (see T&T for a more detailed discussion on formation of tails and bridges). 06206-6315 is a spectacular example of a violent interaction where two (if not three) nuclei are involved, and where there is a hint of an arm or tidal tail to the NE of the two nuclei. Clearly, this system is still in the close interaction phase, with the two nuclei still clearly visible. What is even more interesting is that east of the main interacting nuclei, there is a formation of some kind, perhaps material being torn apart from one of the two main nuclei. A similar case is encountered in 04063-3236. A closely interacting system with a hint of tidal arms running NE-SW of the interacting body. The arm is not

as clearly delineated as in 06206-6315. These two interacting galaxies probably have had a close encounter and they are now orbiting each other. Finally, 23389-6139 and 0019-6139 are examples of systems displaying bridges among the interacting components. It is very likely than in both cases the interaction involves multiple components although the exact stage of the interaction (early or advanced) cannot be inferred easily.

Although it is hard to draw firm statistical conclusions about the interaction stage by looking through the various tidal features that the galaxies display, we can, at least quantify the percentage of ULIRGs at each stage. The results are displayed in Table 7. A small percentage of ULIRGs , $\sim$7%, are fully relaxed systems with no sings of recent interaction. A somewhat larger fraction 22%, has completed the merging process and is probably moving towards a fully relaxed system, still showing however, prominent tails but no second nucleus is visible. 50% or more of ULIRGs are still interacting, since both nuclei can be seen in the images. We can, therefore, use the morphological characteristics displayed by ULIRGs to probe their evolutionary stage.

6. Testing the Evolutionary Scenario for ULIRGs

The QSO equivalent luminosities of ULIRGs led Sanders et al. (1988) to propose an evolutionary scenario in which ULIRGs are the precursors of QSOs. According to this plausible scenario interactions and merging of the ULIRG parent sample cause gas to be transported to the inner parts of the galaxies. This central gas concentration triggers powerful starburst activity. As the merger advances the starburst activity subsides and the gas that accretes onto the nucleus proper creates a new or fuels an existing AGN whose luminosity increases rapidly and dominates the bolometric output during the ULIRG phase. Eventually, all the obscuring dust is shed and the ULIRG develops into a normal QSO.

The obvious prediction of this scenario is that the more advanced mergers should, on average, be more AGN like. In other words there should be a correlation between some indicator of merger advancement (like projected nuclear separation) and some diagnostic that measures the relative contribution of the AGN to the bolometric/IR luminosity. Our mid-infrared spectroscopic survey and in particular the PAH L/C ratio has proven to be a powerful tool (Genzel et al. 1998, Lutz et al. 1998) in measuring the contribution of the AGN to the ULIRG bolometric luminosity. The mid infrared observations and their comparison to optical spectroscopy (Lutz, Veilleux and Genzel 1999) indicate that *part* of the Sanders et al. (1988) scenario is incorrect: most ULIRGs are not buried QSOs. The second part remains to be tested: ULIRG evolution from starburst to AGN may still exist even if the obscured AGN phase is less important. To test the latter part, independent indicators of evolutionary status such as nuclear separations and merger models are required. It is clear that high resolution near-IR imaging data are crucial in determining accurate separations. A first attempt to test this scenario was made by Lutz et al. (1998) where the data for the nuclear separations were taken from the literature. For this incomplete set of data for the nuclear separations Lutz et al. found that there appears to be no trend toward AGN dominance with decreasing separations.

We now combine our new high resolution imaging data, with NICMOS archival data and with data from the samples of Duc, Mirabel and Maza (1997), Graham et al. (1990), Majewski et al. (1993) and Murphy et al. (1996) to obtain nuclear separations for over 50 ULIRGs. In Figure 10 we plot the PAH L/C as a function of nuclear separations. *No obvious correlation is found between the stage of the merger (measured by the nuclear separations) and the dominant energy source (measured by the PAH L/C).* In addition, we find that starburst dominated ULIRGs can be found over the entire range of observed separations from 0.3 kpc up to 15 kpc.

We use the *Student's t-test* to evaluate the differences between the distribution of the separations in ULIRG-AGN and ULIRG-starbursts. For the calculation of the standard error for the difference of the means, $s_{\rm D}$, we have also used the upper limits but have given them a lower weight. We computed the t-value

$t = \frac{x_{mean1} - x_{mean2}}{s_D}$

and found it to be t=0.24. The mean distributions of the ULIRG-starbursts and the ULIRG-AGN are therefore not statistically different (at the 87% confidence level). In other words, the similarity found in the means of the two distributions (of ULIRG-AGN and ULIRG-starburst) is real. This simple statistical test strengthens our conclusion that there is no correlation between the stage of the ULIRG-merger and the dominant luminosity source (AGN or starburst).

So far, we proved that there is no correlation between stage of the merger and the dominant luminosity using the projected nuclear separations. However, we still need to ensure that the absence of correlation is not a projection effect. We mentioned earlier that the mean projected separation of our ISO-ULIRG sample is $\rm d_{mean,proj} = 6.5$ kpc, which will correspond to a real separation $\rm d_{mean,real} = 6.5/\ cos\theta$, where θ is the inclination angle. Since we do not know the exact value of θ for each system we can estimate the

$rms(cos\theta_{\rm average}) = \int_0^{360} rms(cos\theta) d\theta = 0.707$

Therefore, the real mean separation can be as large as 10 kpc.

Let us now take a look at typical distances and timescales throughout the course of a merger. For this purpose we follow the models of Barnes and Hernquist (1996) or the later ones by Dubinski, Mihos and Hernquist 1999 (in what follows we will refer to their model A). What we are interested in is how the distance between the two interacting galaxies changes with time, as the merger proceeds through the various interaction stages. We note

that the timing of the first event is dependent on a number of parameters, such as for instance, how far apart were the two galaxies when the interaction started, and the masses of the progenitor galaxies. After the first close encounter (at t=0) the two interacting galaxies will start drifting apart to a maximum distance of 50 kpc (aphelion) and then approach each other again during the second passage. This phase lasts for about 6×10^8 yrs, at which point the second close passage occurs. From that point onwards the interaction proceeds rapidly. The galaxies will drift apart again, reaching a maximum distance of 16 kpc and then the third and final close passage (after t=7 $\times10^8$ yrs) happens at which point they will merge completely. Our measured (as well as the deprojected) separations are all smaller than $\sim$50 kpc, the distance to the first aphelion determined by model (A) of Dubinski, Mihos and Hernquist (1999), so all of the imaged ULIRGs are in fact closely interacting/merging.

As we have already mentioned, the timescales to the first close passage, the aphelion distance and the total time to complete merger are strongly dependent on a number of parameters such as the initial distance between the two galaxies, their masses, the inclination of their orbits, etc. Although Barnes and Hernquist (1996) present a number of models for various combinations of the parameters we note that the phase space of most parameters is limited. For instance the initial distance of the two interacting systems cannot be very large because then the systems cannot become bounded. Another crucial parameter is the star formation rate (this will determine how quickly the gas will be used up). From the discussion above, we conclude that the dominant luminosity source in ULIRGs in a given time, is most probably determined by local effects such as the compression of the interstellar gas, the fueling of the AGN and to a lesser extend by the state of the merger.

7. Merging and Evolution scenarios for ULIRGs

The highly distorted morphologies of ULIRGs, the high frequency of double nuclei among them together with the results from our simple test on the classical "evolutionary" scenario of Sanders et al. lead to the conclusion that a more detailed insight into the particulars of the merger procedure is more likely to give valuable clues on the issue of the evolution of ULIRGs and the dominant luminosity source.

In a galactic interaction, the transfer or orbital energy through dynamical friction to internal degrees of freedom in the system marks the onset of the merger. The angular momentum of each nucleus is reduced significantly at each close encounter and after a few such close passes the orbits finally become circular and the two nuclei spiral together. The gas in each of the merging galaxies loses angular momentum too, and concentrates towards the central region. At that stage, the gas can be used to fuel an AGN, a starburst or both. However, the time each galaxy spends at each of these steps is not fixed. According to merger modeling (e.g. Mihos 2000) the result of the various close encounters varies. For instance there is the "pre-collision" stage which is relatively short and the interaction is probably mild, the "impact" stage with an even shorter duration but with strong imprints of the interaction on the disk of the galaxies (perhaps formation of tidal tales), the "self-gravitating" stage which leads into a more closely bound interacting system. After the close encounter phase the final merging takes place followed by the final relaxation of the merger.

Based on our PAH L/C database and our high resolution imaging what can we say for the stage of the merging and the dominant energy sources in ULIRGs? The high percentage of double nuclei systems (68%) among ULIRGs gives the first indication that the ULIRG phase is not confined to the latest stages of mergers. 03521+0028 (log L_{IR}=12.46, d_{linear} = 3.42 kpc), is an example of a high luminosity ULIRG, displaying starburst characteristics

(PAH L/C 3.23) where the two nuclei have not yet experienced the final merging. However, its starburst-powered luminosity has reached maximum levels. In Figure 11 we have plotted the nuclear separation as a function of luminosity for the ISO-ULIRG sample. For comparison we have plotted data for a sample of Luminous Infrared Galaxies (LIRGs) from Gao et al. (1996) and Gao and Solomon (1999). We have computed the correlation coefficient (Pearson-C test) for the L_{IR} vs. separation correlation. We find r = -0.15 for 30 ULIRGs (we note that for the computation of the correlation coefficient we have not used data for ULIRGs with upper limit values for the separations). Clearly, this indicates that there is a very weak (not significant) anticorrelation. In other words the ULIRG luminosity stays, on average, about the same at different separations. The most luminous ULIRGs are found over a wide range of separation and *not* just exclusively at the smallest separations. Turning to the LIRGs the computed correlation coefficient of r=0.18 similarly implies a very weak correlation between L_{IR} and separation. Therefore, it seems likely that the maximum activity can be reached at any stage during the merger and not necessarily at the final stages after the merger has been completed. However, this is not what would be expected on the basis of the star formation rate scaling with the average gas density as a Schmidt law $R_\star \propto M_{gas}\ \rho^{\alpha}_{gas}$, $\alpha = 0.5$ –1. Using this parameterization Mihos & Hernquist (1996) predict that most of the star formation events take place in the final merging of two nuclei in a single one.

Mihos and Bothun (1998) reached a similar result by studying the H_α kinematics in four ULIRGs. In their sample they do not see a trend for increased luminosity or, ULIRG activity, in systems with more centrally concentrated H_α. Clearly, the collisions will drive the gas towards the center (where it can fuel an AGN or a starburst) however, the ULIRG phase or the maximum luminosity may happen at any given point in the merging sequence and not in the very final stages when the merger has taken place.

To probe further the relation (if any) between molecular content and stage of merger we have examined the correlations between separation and observed CO luminosity and, separation and star-formation "efficiency" L_{IR}/ M_{H_2}. In both cases we compare the correlations for ULIRGs with those for LIRGs (CO data for ULIRGs and LIRGs are from Gao and Solomon 1999). In Figure 12 we have plotted the nuclear separation as a function of L_{IR}/ M_{H_2}. No correlation is found between L_{IR}/ M_{H_2} and separation for ULIRGs (correlation coefficient r=-0.07). However, a somewhat more significant anticorrelation is found for LIRGs, with a correlation coefficient r=-0.41. This would imply that the star formation rate in LIRGs normalized to the available molecular mass, increases with decreasing separation in agreement with the conclusion of Gao and Solomon (1999).

There is no correlation (Figure 13) between CO luminosity, L_{CO}, and separation for ULIRGs (r=-0.046). We find that for ULIRGs the values of L_{CO} remain almost constant and vary between 0.3×10^{10} $L_\odot$ and 1.6×10^{10} $L_\odot$. Clearly, there is an evident correlation for LIRGs (r=0.61). The correlation indicates that for LIRGs L_{CO} decreases as the merger progresses to advanced stages. We suggest that the difference between ULIRGs and LIRGs in the L_{CO} vs. separation correlation indicates (together with the short starburst timescales discussed in the next paragraph) that the star formation process in major mergers is not terminated by the systems running out of gas reservoir but by the negative feedback of star-formation.

The timescales of the bursts in ULIRGs are estimated to be short, that is no more than a few tens of millions of years in the most luminous systems, and perhaps as small as $5–10\times10^6$ years $\ll t_{merger}$ (Genzel et al. 1998, Goldader et al. 1997, Thornley et al. 1999). These timescales are smaller than the estimated duration of the ULIRG phase, found to be about 10^7–10^8 years. How can the two different timescales be reconciled? The models of Barnes and Hernquist (1996) and Mihos and Hernquist (1996) predict that strong

compression of the interstellar gas happens during or after every 2 or 3 close approaches. Strong gravitational torques remove a large fraction of the angular momentum of the gas which results in the gas being compressed. If star formation follows a Schmidt law then star formation can occur during brief phases over a few dynamical timescales (of the order of a few ten million years) at each close approach (pericenter). An alternative to this would be to appeal to an AGN for the extra luminosity required. The presence of the AGN will shorten the difference in the timescales (duration of the ULIRG phenomenon and burst lifetime). However, only in a few cases does there exist evidence for the presence of an AGN contributing significantly to (although not dominating) the bolometric output. Such cases include for instance UGC5101 (compact IR dust source, Genzel et al. 1998), and Mrk 273 (optical spectroscopy, X-rays, Rigopoulou et al. et al. 1996b).

Although from the present data we cannot exclude the presence of an AGN in ULIRGs, the AGN is definitely in a very "quiet" stage. Also since the occurrence of AGN in single nuclei systems is low there is no proof for an evolutionary scenario in which after the final stages of the merger the system should host an AGN. A clear example of this is 20551-4250 which appears to be a single nucleus, probably having just undergone merging (as evidenced by the presence of tails), yet with a PAH L/C of 2.33. Moreover, its optical spectrum (Kim et al 1998) shows signs of starburst activity.

So what happens to the ULIRG phase? Most likely the ULIRG phenomenon should be attributed to the burst events which are initiated through gas compression in every close approach of the two nuclei. A number of other factors must contribute to the ULIRG phenomenon as well. Based on our high resolution imaging and input from merger models, at this stage, we can only make a list of possible factors contributing to the ULIRG phenomenon. These include the geometry of the encounter, the size of the galaxies and their structures and also the available gas in the two merging disks. As molecular measurements

of ULIRGs have shown (Rigopoulou et al. 1996a, Downes and Solomon 1998) ULIRGs are very gas rich galaxies. The exact geometry of the encounter will determine the number of close approaches. In turn the amount of gas available will regulate the burst events. The individual structure of each galaxy will determine the lifetime of the interaction until final merger and transition to the quiescent stage. Whether or not a black hole will be created or may already have existed in one of the two nuclei, is probably not connected to the ULIRG phenomenon and certainly we have no evidence of such a black hole contributing significantly to the bolometric luminosity.

8. Conclusions

We have presented an atlas of the ISOPHOT-S spectroscopic survey of 62 ULIRGs ($L_{IR} > 10^{12}$ $L_{\odot}$) plus comparison templates of AGN, starbursts and normal galaxies, which was carried out as part of the MPE ISO Central Program. The range covered by the ISOPHOT-S spectra 5-12 μm is the region of the PAH emission features. We use the line-to-continuum ratio of the 7.7 PAH feature to distinguish between AGN and starburst activity.

We find that, on average, ULIRGs exhibit properties resembling those of starbursts. The ratios of PAH over infrared luminosities, L_{PAH}/ L_{IR}, are found to be similar for starburst dominated ULIRGs and template starbursts. We find that extinction severely affects the strength and shape of the PAH features. The PAH spectrum of ULIRGs resembles very much that of an obscured starburst as is demonstrated from a comparison of the spectrum of Arp 220 with that of M82 for which additional extinction has been applied.

As a followup of the ISOPHOT-S ULIRG sample we have obtained high resolution NIR imaging for a complete sample of Southern ULIRGs. The majority of ULIRGs (68%)

appear to contain double nuclei. Among the 23 double nuclei systems 17 of them appear at linear separations between 4-14 kpc, with a mean separation of 6.5 kpc. The presence of tails and bridges in almost all ULIRGs implies that they are undergoing merging. We find that up to 50% of the ULIRGs imaged have not yet experienced the final merging.

An observational test of the Sanders evolutionary scenario shows that there is no trend for advanced mergers to be more AGN-like. In fact we find that the mean distribution of separations between ULIRG-AGN and ULIRG-starburst are similar. We estimate that projection effects are not likely to significantly affect our results. We find that AGN or starburst dominated ULIRGs can be found at all nuclear separations.

Although an AGN and a starburst may concurrently occur in ULIRGs there is no proof for an evolution of the type ULIRG-starburst $\rightarrow$ ULIRG-AGN. The dynamical lifetime of the ULIRG phase could be explained by burst events only. No evidence is found for AGN to dominate even among the fully merged systems. We have found no correlation between infrared luminosity output and merger stage (or separation), a similar behavior is found in a sample of LIRGs studied here as well.

Finally, we propose that the particulars of the merging/interacting nuclei, such as the gas available in the progenitor galaxies and the individual galaxy structure may also determine the merger procedure and the ULIRG evolution.

We are grateful to Andreas Eckart, Volker Springel, and Linda Tacconi for discussions and useful suggestions. We thank the anonymous referee for his/her comments and suggestions. SWS and the ISO Spectrometer Data Center at MPE are supported by DLR (DARA) under grants 50 QI 8610 8 and 50 QI 9402 3. This work has made use of the NASA/IPAC Extragalactic Database which is operated by the Jet Propulsion Laboratory, California Institute of technology, under contract with the National Aeronautics and Space

Administration.

REFERENCES

Acosta-Pulido, J., et al., 1996, A&A 315, L121

Acosta-Pulido, J. 1999, ISO Explanatory Library, in prep.

Armus, L., Heckman, T.M., & Miley, G.K., 1990, ApJ364, 471

Armus, L., Neugebauer, G., Soifer, B.T., and Matthews, K., 1995, AJ110, 610

Barnes, J.E., & Hernquist, L., 1996, ApJ471, 115

Borne, K.D., Bushouse, H., Colina, L., Lucas, R.A., 1998, IAUS, 179, 275

Boulanger F., Boissel P., Cesarsky D., Ryter C. 1998, A&A, 339, 194

Carico, D.P., Graham, J.R., Matthews, K., Wilson, T.D., Soifer, B.T., Neugebauer, G., and Sanders, D.B., 1990, ApJ349, L39

Charmandaris V., et al., 1997, in: "Extragalactic Astronomy in the Infrared", eds. G.A.Mamon, T.X.Thuân, J.Trân Thanh Vân, (Paris: Editions Frontieres), 283

Clements, D.L., Sutherland, W.J., McMahon, R.G., and Saunders, W. 1996, MNRAS279, 477

Condon, J.J., Huang, Z.P., Yin, Q.F., & Thuan, T.X., 1991, ApJ378, 65

Crawford, T., et al., 1996, ApJ460, 225

Cutri, R.M., and McAlary, C.W., 1985, ApJ296, 90

Devillard, N., 1997, "The eclipse software", The messenger No 87 - March 1997

Downes, D., Solomon, P.M., 1998, ApJ507, 615

Draine, B.T., 1989, in Infrared Spectroscopy in Astronomy, ed. B.H. Kaldeich, ESA-SP, p93

Dubinski, J., Mihos, J.C., Hernquist, L., 1999, astro-ph/9902217

Duc, P.-A., & Mirabel, I.F., & Maza, J., 1997, A&AS 124, 533

Dudley C. 1999, astro-ph/9903250

Fisher, K., B., Huchra, J.P., Strauss, M.A., Davis, M., Yahil, A., & Schlegel, D., 1995, ApJS, 100,69

Förster-Schreiber N. 1999, PhD thesis, Ludwig-Maximilians Universität München

Gao, Y., Gruendl, R., Hwang, C.Y., & Lo, K.Y. 1999, in IAU Symp. 186, Galaxy Interactions at Low and High Redshift, ed. J.E. Barnes & D. B. Sanders (Dordrecht: Kluwer), in press

Gao, Y., and Solomon, P.M., 1999, ApJ512, L99

Gabriel, C., Acosta-Pulido, J., Heinrichsen, I., Morris, H., Tai, W.-M. 1997, in Proc. of the ADASS VI conference, ed. G. Hunt & H.E. Payne (San Francisco: ASP), 108

Genzel, R., Witzel, L., Tacconi-Garman, L.E., Blietz, M., Cameron, M., et al., 1995, ApJ444,129

Genzel R., Lutz, D., Sturm, E., Egami, E., Kunze, D., et al., 1998, ApJ498, 579

Gillett F.C., Forrest W.J., Merrill K.M. 197, ApJ, 183, 87

Gillett F.C., Kleinmann D.E., Wright E.L., Capps R.W. 197, ApJ, 198, L65

Goldader, J.D., Joseph, R.D., Sanders, D.B., and Doyon, R., 1997, ApJ474, 104

Graham, J.R., Carico, D.P., Matthews, K., Neugebauer, G., Soifer, B.T., and Wilson, T.D., 1990, ApJ354, L5

Heckman, T.M., Armus, L., & Miley, G.K., 1990, ApJSuppl. 74, 833

d'Hendecourt L., et al. 1996, A&A, 315, L365

Joseph, R.D., & Wright, G.S., 1984, Nature, 311, 132

Kessler, M.F., et al. 1996, A&A, 315, L27

Kii, T., Nakagawa, T., Fujimoto, R., Ogasaka, T., Miyazaki, T., Kawabe, R., and Terashima, Y., 1997, in X-ray Imaging and Spectroscopy of Cosmic Hot Plasmas, eds. F. Makino and K. Mitsuda (Universal Academic Press:Tokyo), 161

Kim, D.C., Sanders, D.B., Veilleux, S., Mazarella, J.M., and Soifer, B.T., 1995, Ap.J.Suppl. 98,129

Kim, D.C., Veilleux, S., & Sanders, D.B., 1998, ApJ508, 627

Lai, O., Rouan, D., Rigaut, F., Arsenault, R., Gendron, E., 1998, A&A 334, 783

Laurent O., Mirabel I.F., Gallais P., Sauvage M., Vigroux L., Cesarsky C., Charmandaris V. 2000, Ap&SS, in press (Proceedings of 1998 Ringberg workshop on ultraluminous infrared galaxies)

Leech, K.J., Rowan-Robinson, M., Lawrence, A., and Hughes, J.D., 1994, MNRAS267, 253

Lemke, D., et al. 1996, A&A, 315, L64

Lonsdale, C.J., Smith, H.E., & Lonsdale, C.J., 1993, ApJ405, L9

Lutz, D., et al. 1996, A&A 315, L269

Lutz, D., Spoon, H.W.W., Rigopoulou, D., Moorwood, A.F.M., and Genzel, R., ApJ505, L103

Lutz, D., Veilleux, S., Genzel, R., 1999, ApJ517, L13

Majewski, S.R., Hereld, M., Koo, D.C., Illingworth, G.D., and Heckman, T.M., 1993, ApJ402, 125

Mattila K., Lehtinen K., Lemke D. 1999, A&A, 342, 643

Mattila, K., et al. 1996, Astr.Ap. 315, L353

Mihos, J.C., & Hernquist, L., 1996, ApJ464, 641

Mihos, J.C., & Bothun, G.D., 1998, ApJ500, 619

Mihos, J.C., 2000, Ap&SS, in press (Proceedings of 1998 Ringberg workshop on ultraluminous infrared galaxies)

Moorwood A.F.M. 1986, A&A, 166, 4

Moorwood, A.F.M., et al., 1996, A&A315, L109

Moorwood, A., Cuby, J.-G., Lidman, C. 1998, The Messenger, 91,9

Murphy, T.W., et al., 1996, AstronJ, 111(3), 1025

Noguchi, M., 1991 MNRAS251, 360

Ogasaka, Y., et al., 1997, PASJ 49, 179

Pier E.A., Krolik J.H. 1992, ApJ, 401, 99

Puget, J-L., Léger, A., 1989, Ann.Rev.Astr.Ap. 27,161

Rigopoulou, D., et al., 1996a, A&A 305, 747

Rigopoulou, D., Lawrence, A., & Rowan-Robinson, M., 1996b, MNRAS278, 1049

Rigopoulou, D., et al. 1999 in prep

Roche, P.F., Aitken, D.K., Smith, C.H., and Ward, M.J. 1991, MNRAS248, 606

Roelfsema P.R., et al. 1996, A&A, 315, L289

Roelfsema P.R., Cox P., Kessler M.F., Baluteau J.-P. 1998, in: "Star Formation with the Infrared Space Observatory", eds. J.L. Yun and R. Liseau, ASP Conf. Series 132, 76

Rowan-Robinson, M., Crawford, J., 1989, MNRAS263, 675

Sanders, D.B., et al., 1988, ApJ325, 74

Sanders, D.B., & Mirabel, I.F., 1996, ARA&A, 34, 725

Sakata, A., Wada, S., Onaka, T., and Tokunaga, A., 1987, ApJ320, 63

Smith C.H., Aitken D.H., Roche P.F. 1989, MNRAS, 241, 425

Soifer, B.T., Houck, J.R., and Neugebauer, G., 1987, Ann.Rev.Astr.Ap. 25, 187

Solomon, P.M., Downes, D., Radford, S.J.E., & Barrett, J.W., 1997, ApJ487, 144

Strauss, M.A., Yahil, A., Davis, M., Huchra, J.P., Fisher, K.B., and Tonry, J., 1992, ApJS, 83, 29

Thornley, M.D., et al. 1999, in prep

Toomre, A., & Toomre, J., 1972, ApJ, 178, 623

Tran Q.D., et al. 1999, in prep.

Verstraete, L., et al. 1996, Astp.Ap. 315, L93

Willner S.P., Soifer B.T., Russell R.W., Joyce R.R., Gillett F.C. 1977, ApJ, 217, L121

Whittet D.C.B., et al. 1996, A&A, 315, L357

This manuscript was prepared with the AAS LaTeX macros v4.0.

FIGURES

Fig. 1.— Near-infrared images for the 27 Southern ULIRGs presented here. The images are arranged according to increasing nuclear separation. The K_s band images are plotted in grey scale and contour forms. The faintest contours correspond to 20.5 mag/$\Box''$. Angular scale on the sky is indicated by the bar which represents 10 kpc, except for 05189-2524 for which the bar represents 5 kpc.

Fig. 2.— ISOPHOT-S spectra for the ISO-ULIRGs. The assumed continuum around the PAH features is shown as a straight line. In case of upper limits the Gaussian used to estimate the upper limit is shown. No continuum fit for 09463+8141 (see note 1d).

Fig. 3.— ISOPHOT-S spectra for the ISO-AGN (continuum and upper limits as in Fig.2).

Fig. 4.— ISOPHOT-S spectra for the ISO-starburst, except for M82 where part of an SWS AOT1 spectrum is presented (continuum and upper limits as in Fig. 2).

Fig. 5.— Histograms showing the distribution of the $L_{PAH}/\ L_{IR}$ ratio for ULIRG-starbursts and template starbursts.

Fig. 6.— Illustration of the effect of extinction on PAH spectra. The top panel shows the spectrum of the starburst M 82, as observed and assuming additional screen extinction of A_V=20 and 50. The features at 6.2, 8.6, and 11.3μm are suppressed relative to the one at 7.7μm to which the fluxes have been scaled for clarity. The lower panel shows the spectrum of Arp 220, ressembling an obscured starburst. The PHT-S long wavelength cutoff masks the fact that the 11.3μm feature of Arp220 is placed on a relatively stronger continuum.

Fig. 7.— The 6.2/7.7 PAH ratio is plotted against screen extinction A_V from independent SWS spectroscopy (Genzel et al. 1998)

Fig. 8.— Projected nuclear separation as a function of redshift for the ISO-ULIRGs. Open

squares denote ULIRGs with measured nuclear separations, limits denote ULIRGs with single nuclei (or unresolved doubles)

Fig. 9.— Histogram of the log of the projected linear separation (in kpc) for the Southern ISO-ULIRGs. The hatched area represents the galaxies with upper limits in the their measured nuclear separations.

Fig. 10.— 7.7 PAH L/C as a function of nuclear separation of the interacting components of a ULIRG. Open symbols indicate AGN-ULIRGs, either according to our classification or where there is evidence of an AGN from observations as other wavelengths (although it may not dominate the bolometric luminosity). Filled symbols indicate starburst-ULIRGs. The dashed line indicated the adopted separation between starbursts and AGN at L/C = 1

Fig. 11.— Infrared luminosity L_{IR} as a function of projected nuclear separation. Filled squares and upper limits correspond to our ISO-ULIRG sample. Open squares are data for LIRGs taken from Gao et al. (1996) and Gao and Solomon (1999)

Fig. 12.— Star formation efficiency L_{IR}/ M_{H_2}, as a function of projected nuclear separation.Filled squares and upper limits correspond to our ISO-ULIRG sample. Open squares are data for LIRGs taken from Gao et al. (1996) and Gao and Solomon (1999). Data for ULIRGs from Solomon et al. (1998) and Gao and Solomon (1999)

Fig. 13.— CO luminosity L_{CO} as a function of projected nuclear separation.Filled squares and upper limits correspond to our ISO-ULIRG sample. Open squares are data for LIRGs taken from Gao et al. (1996) and Gao and Solomon (1999). Data for ULIRGs from Solomon et al. (1998) and Gao and Solomon (1999)

Table 1. ISO ULIRGs - PHOT-S Spectroscopy

IRAS Name	cz km/s	L_{IR} $L_\odot$	$Cont_{5.9}$ x10^{-2}Jy	$Cont_{7.7}$ x10^{-2} Jy	$F_{7.7}$[1a] x10^{-2} Jy	Line/Cont
23578-5307	37458	12.11	: 0.00[1b]	0.00	<1.36	NA(0.0)
00153+5454	33448	12.10	1.13	1.73	5.77	3.340(0.821)
0019-7426	28891	12.25	:0.00	: 0.00	< 1.51	NA (0.000)
00262+4251	27800	12.02	0.56	1.46	5.93	4.063 (1.444)
00397-1312	78461	12.77	6.44	9.88	< 2.26	< 0.229 (0.000)
01003-2238	35286	12.19	1.40	0.37	3.10	1.441 (0.385)
01166-0844	35437	11.99	: 0.14	0.84	< 1.81	< 2.161 (0.000)
01199-2307	46887	12.21	: 0.07	: 0.74	2.08	> 0.971 (0.000)
01298-0744	40826	12.28	1.12	2.07	3.11	1.503 (1.027)
01355-1814	57410	12.39	: 0.028	< 1.81	:0.018	NA (0.000)
01388-4618	27068	12.03	1.12	1.72	6.77	3.938 (0.713)
01494-1845	47007	12.18	: -0.70	: -0.70	3.60	> 1.951 (0.000)
Mrk 1014	48900	12.50	2.52	3.87	<2.42	< 0.626 (0.000)
01569-2939	42030	12.14	: 0.14	1.24	1.42	1.149 (0.398)
02364-4751	29473	12.10	0.7	1.45	5.06	3.490 (0.736)
02411+0354	43051	12.15	0.84	1.49	4.73	3.174 (0.703)
03158+4227	40288	12.51	1.54	2.36	4.09	1.729 (0.393)
04063-3236	32949	11.97	0.46	0.89	2.28	2.553 (1.203)
04103-2838	35400	12.13	1.54	2.36	3.26	1.378 (0.337)
04114-5117	37345	12.16	0.28	0.93	< 9.06	< 0.975 (0.000)
06009-7716	35070	11.95	0.31	0.95	3.44	3.632 (1.105)
06035-7102	23823	12.14	4.89	7.51	8.32	1.108 (0.258)
06206-6315	27713	12.14	1.23	1.44	5.31	3.687 (2.206)
06301-7934	46891	12.28	: 0.14	: 0.34	< 1.06	NA (0.000)
06361-6217	47967	12.28	1.40	2.15	1.45	0.676 (0.258)
UGC 5101	12000	11.94	5.90	8.78	18.6	2.123 (0.346)
09463+8141[1d]	46378	12.20				
12112+0305	21788	12.25	1.68	2.58	8.08	3.135 (0.634)
Mrk 231	12660	12.48	60.6	91.9	28.9	0.314 (0.021)
Mrk 273	11132	12.07	7.62	10.1	19.3	1.908 (0.322)
14348-1447	24732	12.27	1.26	1.93	6.86	3.550 (0.797)
15250+3609	16000	11.95	2.80	4.45	12.8	2.880 (0.695)
Arp 220	5450	12.11	7.00	9.84	41.4	4.205 (0.447)
16334+4630	57265	12.34	:0.28	: 0.28	< 1.21	NA (0.000)
16474+3430	33418	12.10	0.98	1.58	5.66	3.586 (0.657)
16487+5447	31293	12.11	0.28	0.88	1.93	2.196 (1.111)

Table 1—Continued

IRAS Name	cz km/s	L_{IR} $L_\odot$	$Cont_{5.9}$ $x10^{-2}$Jy	$Cont_{7.7}$ $x10^{-2}$ Jy	$F_{7.7}$[1a] $x10^{-2}$ Jy	Line/Cont
NGC 6240	7339	11.78	10.4	16.2	42.0	2.586 (0.238)
17028+5817	31779	12.09	0.32	1.01	3.60	3.580 (1.087)
17068+4027	53700	12.27	0.69	1.24	1.75	1.409 (0.583)
17179+5444	44211	12.16	0.70	1.20	< 1.66	< 1.386 (0.000)
17208-0014	12900	12.33	3.22	4.94	27.4	5.549 (1.006)
18443+743	40395	12.22	0.98	1.48	2.53	1.708 (0.550)
18470+3233	23626	12.01	: 0.00	: 0.00	< 0.651	NA (0.000)
18531-4616	42202	12.17	0.42	1.02	2.65	2.597 (1.283)
19254-7245	18500	12.02	7.00	9.50	8.46	0.891 (0.175)
19420+4556	35356	11.99	0.28	67.9	2.51	3.698 (2.024)
19458+0944	29980	12.28	0.70	1.55	3.79	2.447 (1.150)
20049-7210	37893	11.93	: 0.00	0.35	1.32	3.771 (2.448)
20100-4156	38848	12.55	1.40	2.15	4.14	1.926 (0.707)
20446-6218	32078	12.04	: 0.00	: 0.5	< 2.11	NA (0.000)
20551-425	12788	11.98	4.53	6.96	16.3	2.339 (0.458)
21396+3623	42000[1e]	11.99	0.64	1.31	3.04	2.311 (0.615)
22055+3024	38041	12.15	: 0.28	: 0.68	< 1.97	NA (0.000)
22491-1808	23170	12.11	0.84	1.54	4.39	2.854 (1.603)
23060+0505	52200	12.41	9.10	14.0	< 1.21	< 0.087 (0.000)
23129+2548	53700	12.38	0.42	0.52	1.85	3.552 (1.928)
23128-5919	13371	11.96	4.17	6.40	18.4	2.870 (0.504)
23230-6926	31870	12.22	: 0.42	: 0.42	< 3.78	NA (0.000)
23253-5415	38838	12.26	0.31	:0.35	1.66	> 1.588 (0.000)
23327+2913	32000	12.04	: 0.14	: 0.59	<2.27	NA(0.0)
23365+3604	19340	12.09	1.26	1.93	8.66	4.479(1.055)
23389-6139	27806	12.10	: 0.42	: 0.42	2.89	> 1.334(0.000)

[1a]7.7 PAH mean peak flux

[1b]: the derived 5.9 μm or 7.7 μm continuum values are within 3 σ from zero

[1c]NA: the 7.7 μm L/C cannot be defined

[1d]The 7.7 μm PAH feature is present. However, no PAH continuum estimates since the off position contains a star which contaminates all background measurements

[1e]velocity derived from PAH features (inconsistent with cz value of 29304 km/s quoted by Strauss et al. (1992)

Note. — Column (1): source name, column (2): velocity cz, column (3): L_{IR} luminosity (see text), column (4): continuum at 5.9 μm, column (6): continuum at 7.7 μm, column (7): 7.7μm PAH peak flux, column (8): line-to-continuum ratio of the 7.7 μm PAH emission feature and error (in parentheses).

Table 2. ISO AGN - PHOT-S Spectroscopy

Name	cz km/s	L_{IR} $L_\odot$	$Cont_{5.9}$ x10^{-2}Jy	$Cont_{7.7}$ x10^{-2} Jy	$F_{7.7}$[2a] x10^{-2} Jy	Line/Cont
IZw1	18342	11.87	17.3	22.1	<4.85	<0.219(0.0)
Mrk 1	4780	10.53	2.09	8.83	<2.71	<0.307(0.0)
NGC 1068	1148	11.29	866	145	233	0.161(0.018)
4U0241+62	13200	11.44	24.5	30.7	<2.86	<0.093(0.0)
NGC 1275	5264	11.21	11.5	21.4	<3.76	<0.176(0.0)
NGC 1365	1636	11.07	55.9	96.6	221	2.290(0.129)
PG0804+761	30000	11.52	7.14	7.02	<1.21	<0.172(0.0)
NGC 3783	2550	10.39	20.7	28.3	<3.61	<0.128(0.0)
NGC 4151	995	10.20	88.2	109	<8.45	<0.077(0.0)
3C273	47500	12.69	18.5	19.6	<2.43	<0.124(0.0)
M 87	1282	8.84	10.2	7.03	<1.51	<0.214(0.0)
CenA	547	9.98	100	122	153	1.258(0.066)
Mrk 463	14904	11.71	23.8	29.8	6.27	0.211(0.034)
Circinus	436	9.87	450	623	1002	1.630(0.062)
NGC 5506	1853	10.36	64.6	71.3	31.2	0.437(0.032)
NGC 5643	1199	10.25	7.1	17.8	11.5	0.645(0.122)
PG1613+658	38700	11.91	3.92	6.02	<1.06	<0.176(0.0)
PG1700+518	87600	12.59	3.5	3.75	<1.97	<0.524(0.0)
PKS2048-57	3402	10.79	23.8	43.3	<6.07	<0.140(0.0)
HB21219-1757	33900	12.04	6.46	9.91	<1.51	<0.152(0.0)
PG2130+099	18630	11.36	8.02	9.41	<1.81	<0.193(0.0)
NGC 7469	4892	11.56	27.4	53.9	53.8	0.997(0.061)
NGC 7582	1575	10.80	33.2	50.9	127	2.484(0.158)

[2a]7.7 PAH mean peak flux

Note. — Column (1): source name, column (2): velocity cz, column (3): L_{IR} luminosity (see text), column (4): continuum at 5.9 μm, column (6): continuum at 7.7 μm, column (7): 7.7μm PAH peak flux, column (8): line-to-continuum ratio of the 7.7 μm PAH emission feature and error (in parentheses).

Table 3. ISO starbursts - PHOT-S Spectroscopy

IRAS Name	cz km/s	L_{IR} $L_\odot$	$Cont_{5.9}$ x10^{-1}Jy	$Cont_{7.7}$ x10^{-1} Jy	$F_{7.7}$[3a] x10^{-1} Jy	Line/Cont
NGC 253	245	10.44	15.6	33.1	100	3.018(0.192)
IC 342	34	9.56	4.35	9.80	27.7	2.826(0.190)
M 82[3b]	203	10.56	35.8	67.8	284	4.195(0.110)
NGC 3256	2738	11.55	4.45	7.89	33.0	4.183(0.243)
NGC 4945	560	10.20	8.33	7.34	78.4	10.69(0.827)
M 83	516	9.81	6.24	13.9	44.4	3.194(0.245)
NGC 5253	404	9.29	3.29	5.44	2.71	0.498(0.047)
NGC 6764	2416	10.36	0.406	1.06	1.38	1.303(0.180)
NGC 6946	48	9.83	2.83	4.25	22.7	5.350(0.357)
NGC 7552	1585	10.99	3.77	7.68	22.2	2.885(0.189)
NGC 891[3c]	528	9.84	1.61	1.80	7.26	4.023(0.277)
M 81	-34	8.58	3.75	2.91	<0.34	<0.115(0.00)
M 51[3c]	463	9.75	1.01	1.70	2.39	1.411(0.149)
NGC 4569[3c]	-235	9.90	0.82	1.46	1.86	1.276(0.185)

[3a]7.7 PAH mean peak flux

[3b]SWS AOT1 spectrum

[3c]Normal Galaxies

Note. — Column (1): source name, column (2): velocity cz, column (3): L_{IR} luminosity (see text), column (4): continuum at 5.9 μm, column (6): continuum at 7.7 μm, column (7): 7.7μm PAH peak flux, column (8): line-to-continuum ratio of the 7.7 μm PAH emission feature and error (in parentheses).

Table 4. Comparison of the Averaged Spectra

	$Cont_{5.9}$ [4a] x10^{-2}Jy	$Cont_{7.7}$ x10^{-2} Jy	$F_{7.7}$ x10^{-2} Jy	Line/Cont
ULIRGs	0.4	0.61	1.27	2.061(0.103)
starbursts	0.5	0.93	2.77	2.983(0.161)
AGN	7.82	8.76	0.4	0.212(0.003)

[4a] 5.9 μm continua relative to the 60 μm flux

Note. — For the *averaged* AGN spectrum the following galaxies were used: IZw1, Mrk 1, NGC 1068, NGC 1275, NGC 3783, NGC 4151, 3C273, MRK 463, NGC 5506, NGC 5643, PG1613+658, PG1700+518, PKS2048–57, HB21219-1757, PG2130+099

The following galaxies contribute to the *averaged* starburst spectrum: NGC 253, IC342, M82, NGC 3256, NGC 4945, M83, NGC 5253, NGC 6946, NGC 7552

Table 5. ISO ULIRGs - Infrared imaging

IRAS Name	m_K	m_J	Ap(")	Sep(")	Sep(kpc)	Clas	Notes
23578–5307	13.24	14.92	10	<0.7	<1.4	merger completed	1
F00183–7111	14.43	16.27	10	<1.0	<3.8	merger completed	1
00188–0856N[5a]	12.96	15.05	5				2
00188–0856S	14.73	15.92	5				2
00188–0856	12.65	14.49	16	7.0	14.0	interacting	1
0019–7426N	12.38	14.03	5				2
0019–7426S	15.05	16.82	5				2
0019–7426	12.13	13.76	16	7.9	12.5	interacting	1
00397–1312	13.99	16.04	10	<0.7	<2.5	merger completed	1
00406–3127	15.00	16.25	10	<0.9	<3.5	merger completed	1
01003–2238	14.10	15.83	10	<0.5	<1.9	relaxed	1
01166–0844W	14.68	16.35	3				2
01166–0844E	14.93	16.52	3				2
01166–0844	13.7	15.16	12	4.9	9.2	interacting	1
01199–2307	14.69	16.07	10	<0.7	<1.7		1
01298–0744	14.28	15.99	10	<0.8	<1.6	merger completed	1
01355–1814[5b]	14.22		10	2.1	5.8	interacting	1
01388–4618	12.23	13.32	10	<0.8	<1.3		1
01494–1845N	13.87	15.86	2				2
01494–1845S	16.27	18.15	2				2
01494–1845	13.42	15.18	10	3.8	8.9	interacting	1
02411+0354 W	14.49	15.97	1.5				1
02411+0354 Main	14.24	15.86	1.5				2
02411+0354 S	14.97	16.46	1.5				2
02411+0354	12.67	14.37	12	3.2	7.0	interacting	1
F02455–2220	14.63	16.34	10	2.0	7.3	merger completed	1
03521+0028 W	14.76	16.74	1.0				2
03521+0028 E	15.29	16.92	1.0				2
03521+0028	13.63	15.32	10	1.5	3.4	interacting	1
04063–3236 SW	14.93	16.22	1.5				2
04063–3236 NE	14.25	16.02	1.5				2
04063–3236	13.45	14.83	10	2.7	4.9	interacting	1
04114–5117 E	14.19	15.90	2				2
04114–5117 SW	15.12	16.39	2				2
04114–5117	13.58	14.70	10	3.5	6.8	interacting	1

Table 5—Continued

IRAS Name	m_K	m_J	Ap(")	Sep(")	Sep(kpc)	Clas	Notes
05189–2524	10.14	12.62	10	<0.5	<0.38	relaxed	1
06009–7716W	14.19	15.40	2				2
06009–7716E	14.78	15.69	2				2
06009–7716	13.36	14.45	10	3.5	6.5	interacting	1
06206–6315SW	13.64		1.5				2
06206–6315NE	14.46		1.5				2
06206–6315	12.60		10	2.7	4.2	interacting	1
06301–7934	13.64	15.39	15	<0.7	<1.7		1
20049–7210	14.08	15.01	10	<0.8	<1.5		1
20446–6218N	13.21	14.61	3				2
20446–6218S	14.96	15.86	3				2
20446–6218	12.54	13.71	15	5.5	9.5	interacting	1
23253–5415	12.75	13.58	12	<1.4	<2.8	merger completed	1
23389–6139S	13.68	15.28	3				2
23389–6139N	16.82	16.12	3				2
23389–6139	13.13	14.45	10	5.5	8.5	interacting	1
23529–2119	14.48	16.68	10	<0.7	<3.2	merger completed	1

[5a]the double nuclei are distinguished by their orientation on the images, north, south etc.

[5b]K_s integration time : 8 mins

Note. — 1: For single nuclei objects magnitudes are quoted for a 10" aperture.
2: For double nuclei objects magnitudes are quoted for the two nuclei separately: usually the magnitude for each nucleus is determined through a 5" or 3" apertures. The total magnitude quoted for double-nuclei systems corresponds to apertures of 10" or 12" or 16" (depending on the sizes of the objects).

Note. — Column (1): source name, columns (2)-(3): K_s and J magnitudes, column (4): the aperture used to derive the magnitudes, column (5)-(6): angular(") and linear (kpc) separations, column(7):ULIRG interaction stage classification (see section 5.2), column (8): notes for the derived magnitudes.

Table 6. ISO ULIRGs - additional separations

IRAS Name	Sep(")	Sep(kpc)	Ref
00153+5454	4.5	8.08	Murphy
01569-2939	3.75	8.09	Duc
03158+4227	<0.5	<1.0	Murphy
03538-6432	0.6	2.2	NICMOS
06035-7102	5.6	7.5	NICMOS
06361-6217	<0.2	<0.6	NICMOS
UGC 5101	<0.8	0.6	Carico
12112+0305	3.0	3.7	Carico
Mrk 231	<0.2	<0.2	Lai
Mrk 273	1.1	0.7	Majewski
14348-1447	3.4	4.7	Carico
15250+3609	<0.4	<0.4	Majewski
Arp 220	0.9	0.3	Graham
16334+4630	4.4	12.0	Gao
16474+3430	3.6	6.5	Murphy
16487+5447	3.1	5.3	Murphy
17028+5817	13.0	22.0	Murphy
17208-0014	<0.8	<0.6	Murphy
18443+7433	<0.8	<1.7	Murphy
19254-7245	7.8	8.4	Duc
20100-4156	2.7	5.6	NICMOS
20551-4250	<1.2	<0.9	NICMOS
21396+3623	6.7	10.0	Murphy
22491-1808	1.6	2.1	Carico
23128-5919	4.9	3.9	NICMOS
23230-6926	0.6	1.04	NICMOS

Note. — column (1): source name, column (2)-(3): angular(") and linear (kpc) separation, column (4): references, Carico: Carico et al. 1990, Duc: Duc, Mirabel, Maza 1997, Gao: Gao and Solomon 1999, Graham: Graham et al. 1990, Lai: Lai et al. 1998, Majewski: Majewski et al. 1993, Murphy: Murphy et al. (1996), NICMOS: NICMOS archive (Borne et al.)

Table 7. ISO ULIRGs - Interaction Stages

	Fully Relaxed	Merger Completed	Interacting Pairs
Number of galaxies	2	6-7	12
Percentage	7.4%	22%	47%

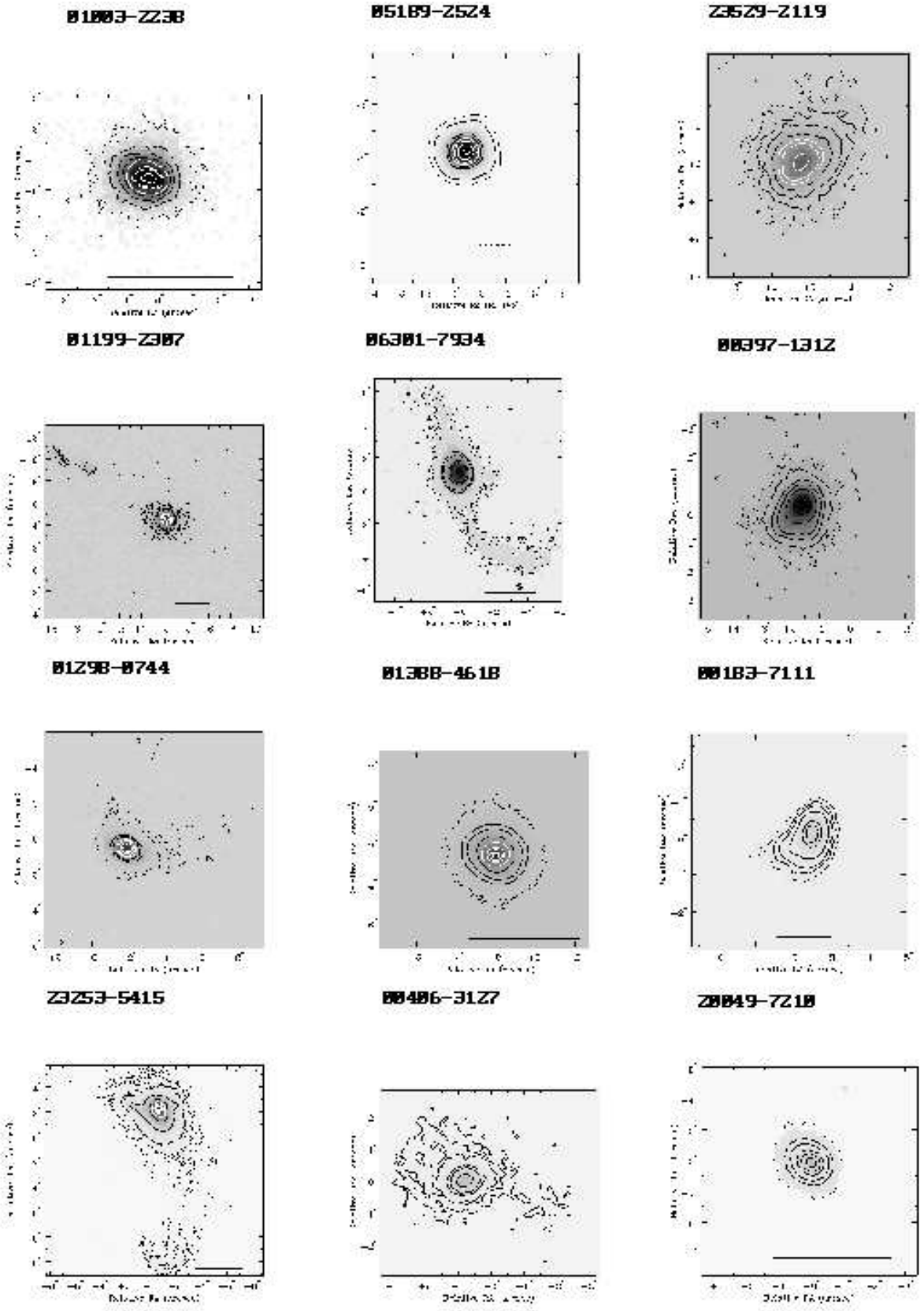

Fig. 1.— K contours

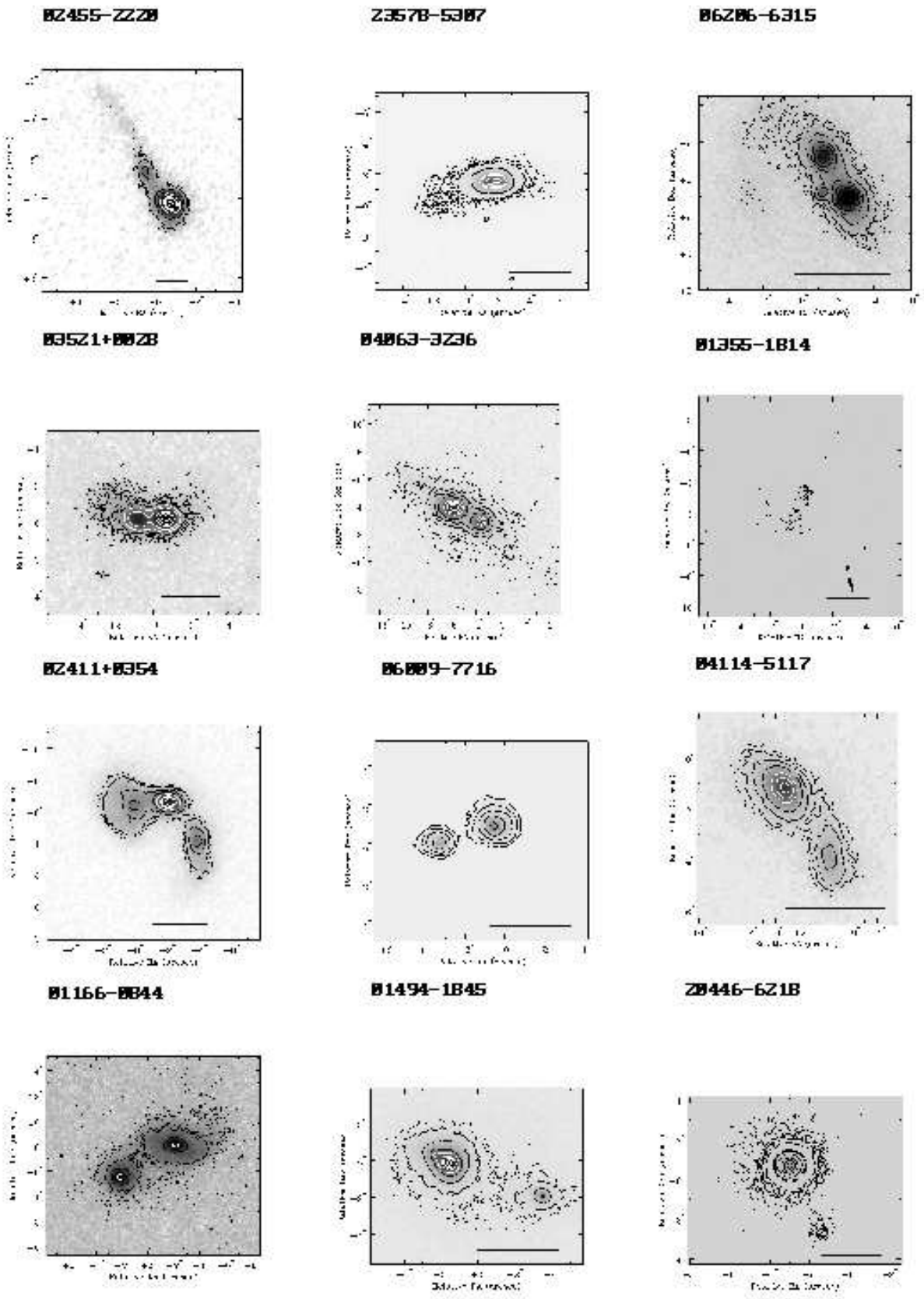

Fig. 1.— K contours, continued

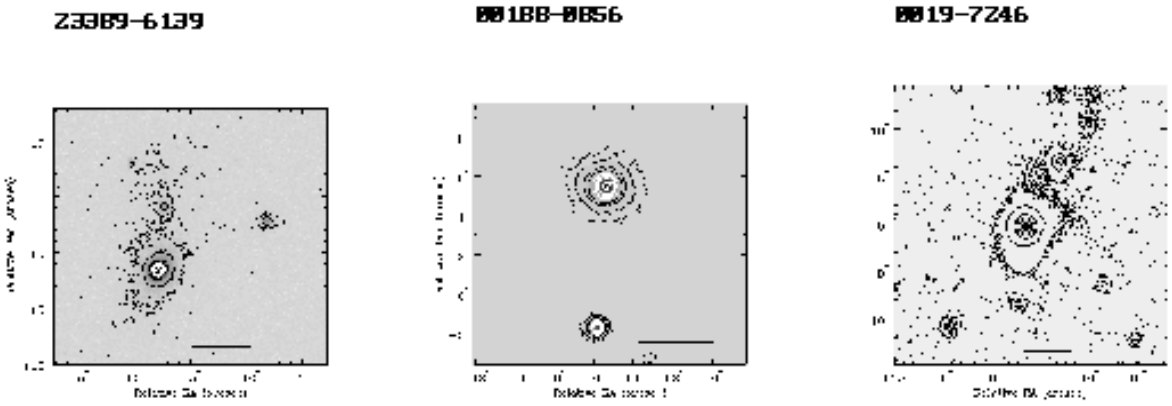

Fig. 1.— K contours, continued

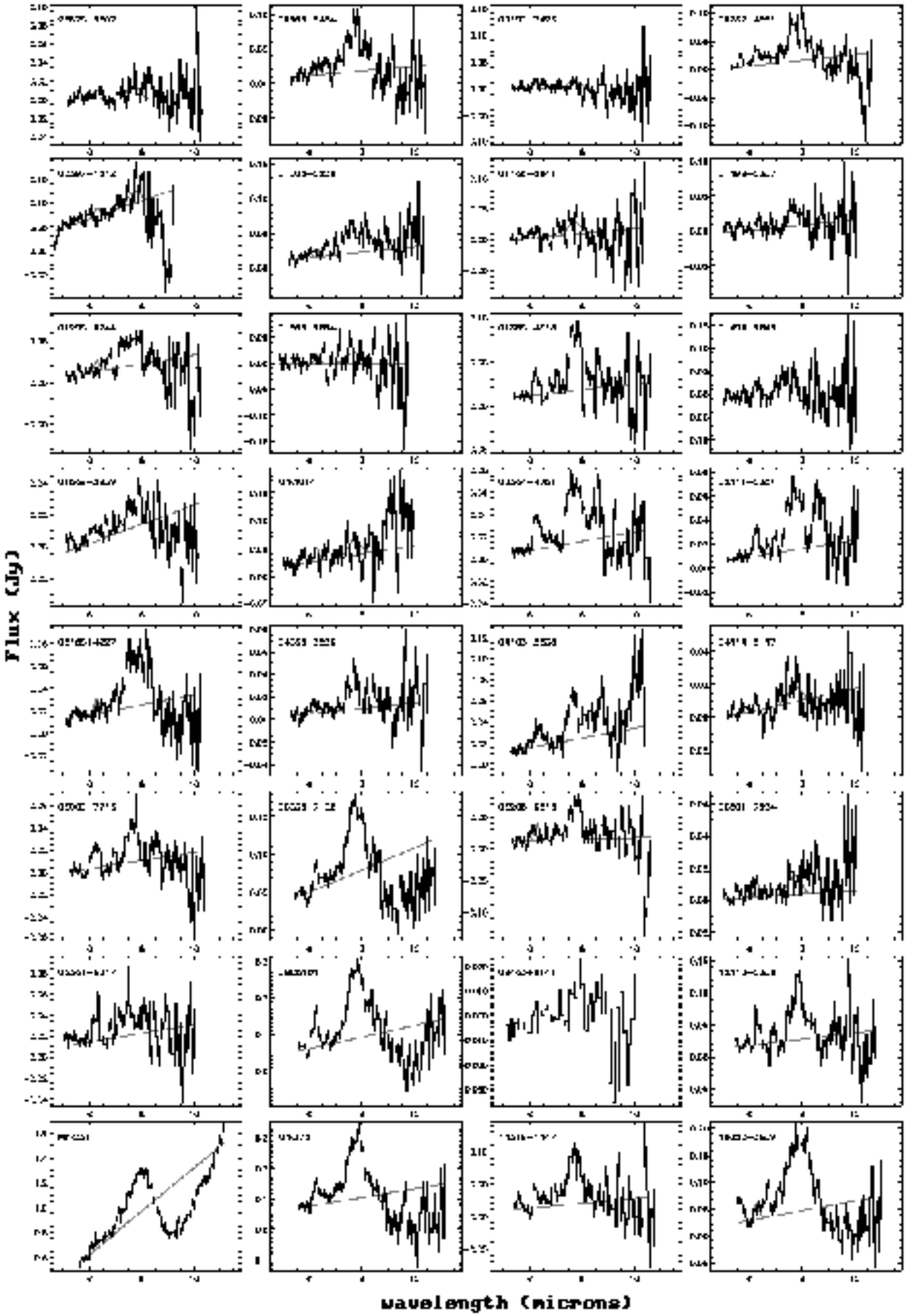
Flux (Jy)
Wavelength (microns)

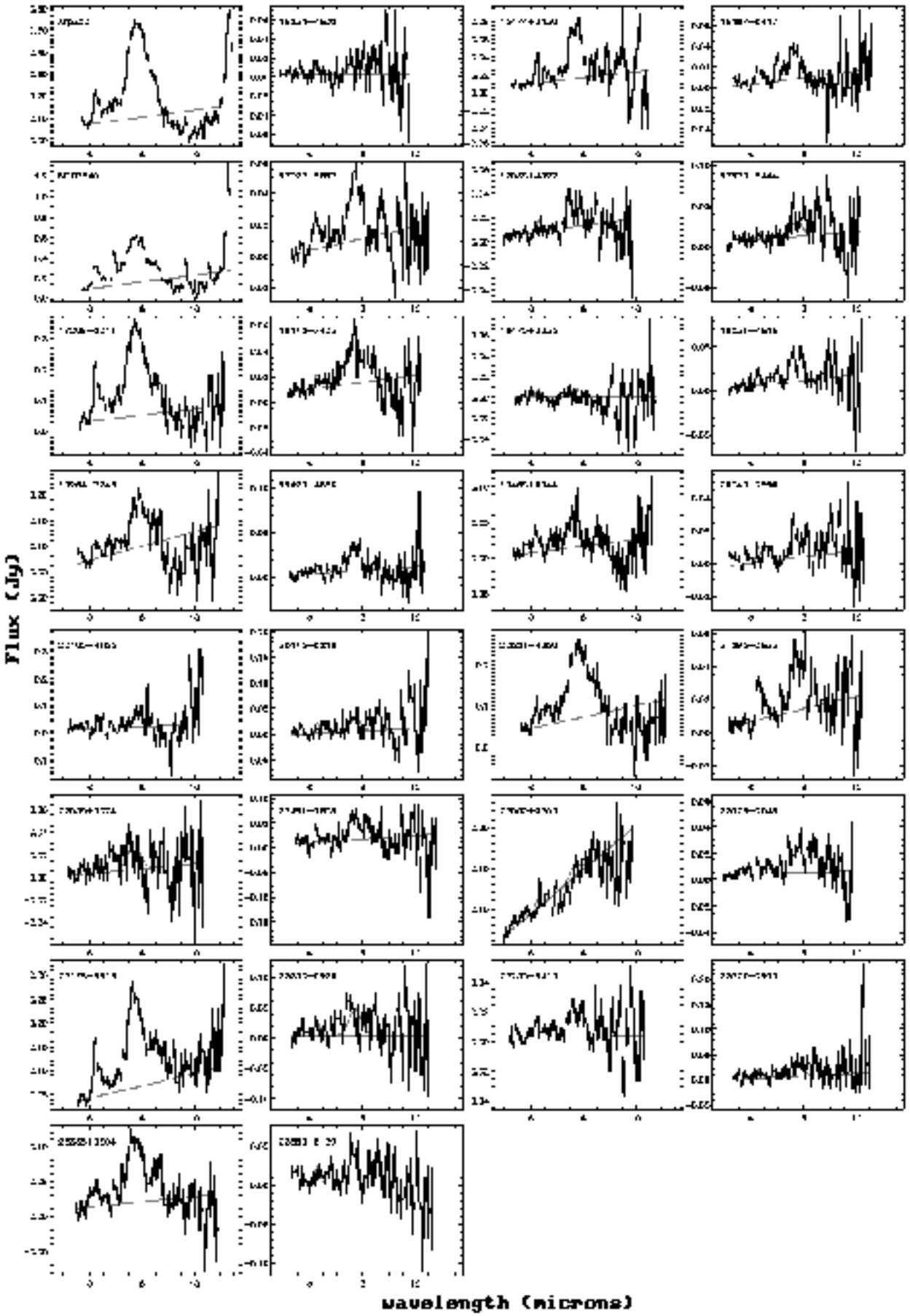
Flux (Jy)
Wavelength (microns)

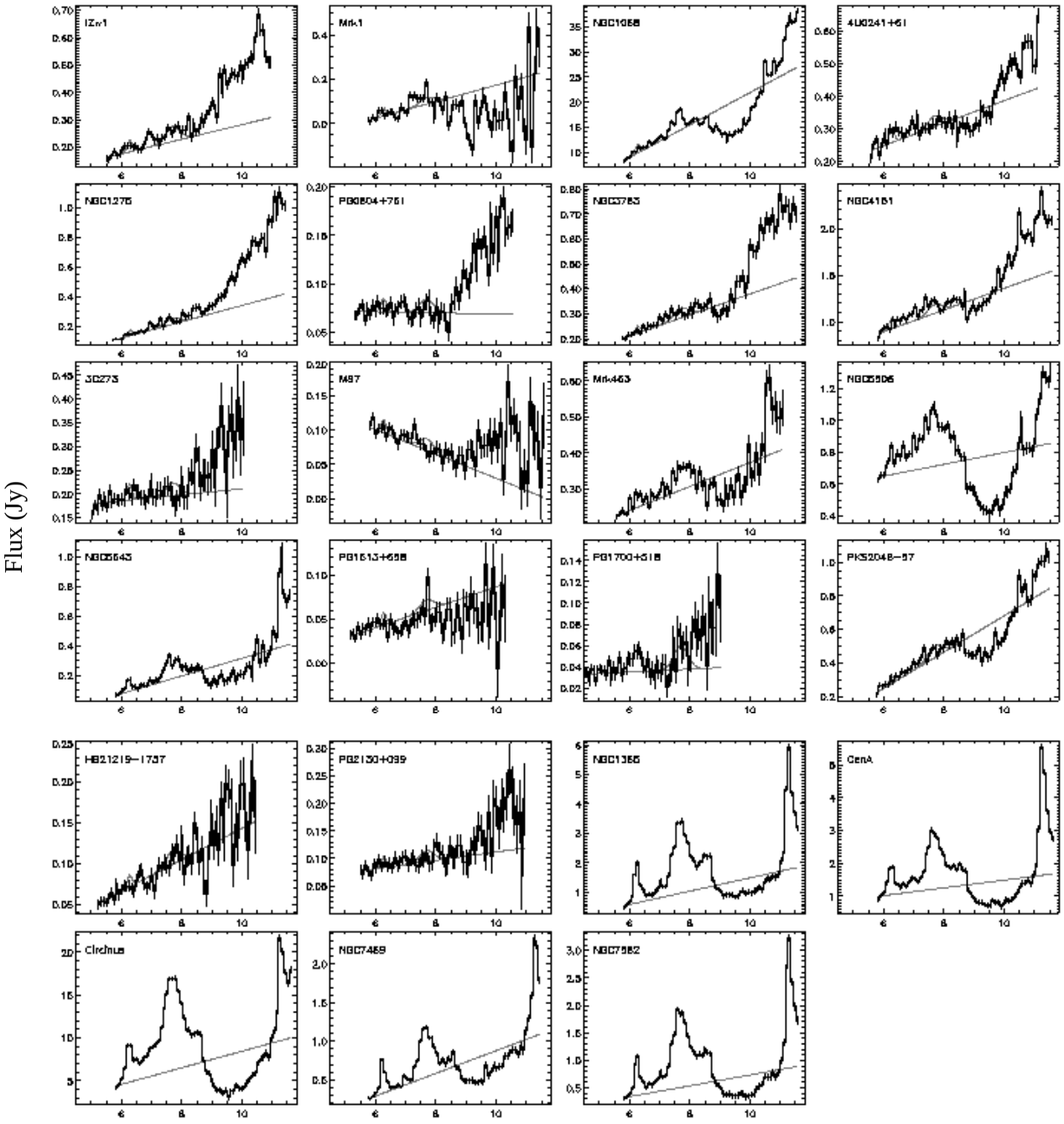
IZw1
Mrk1
NGC1068
4U0241+61
NGC1275
PG0804+761
NGC3783
NGC4151
3C273
M87
Mrk463
NGC5506
NGC5548
PG1613+658
PG1700+518
PKS2048−57
HB21219−1757
PG2130+099
NGC1365
CenA
Circinus
NGC7469
NGC7582
Flux (Jy)
wavelength (microns)

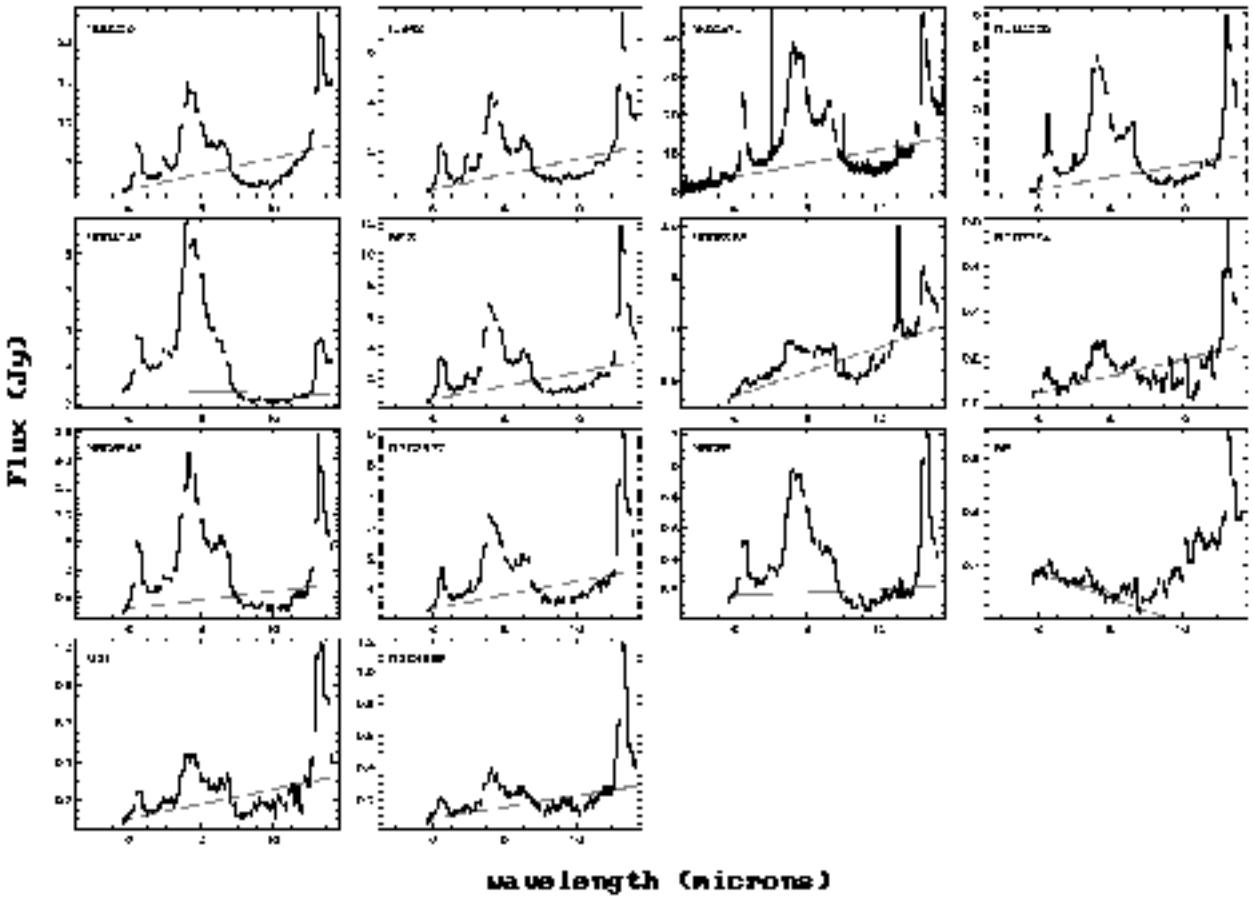

Fig. 4.— ISOPHOT-S Spectroscopy, starbursts

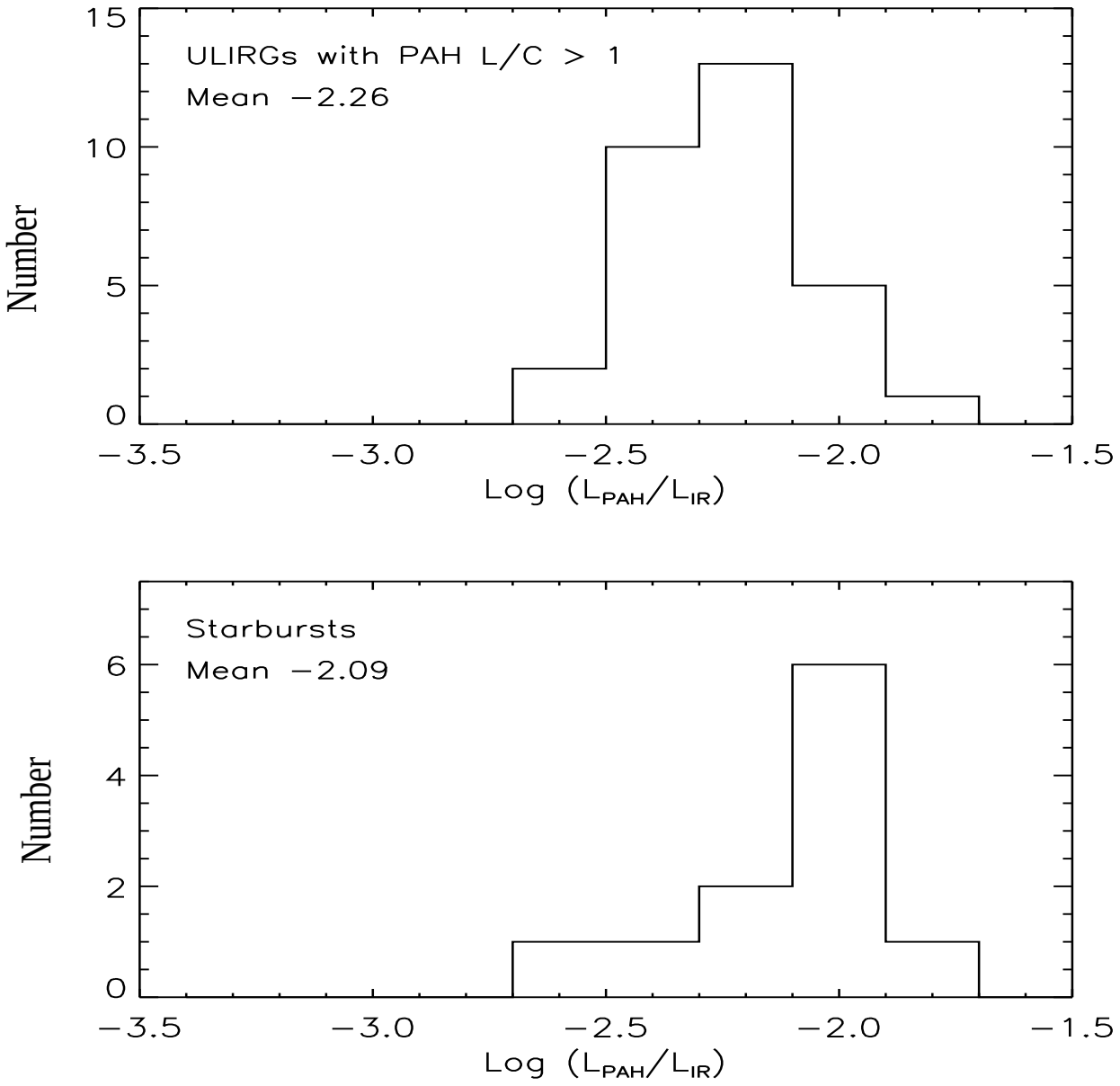

Fig. 5.— Comparison between ULIRG-starbursts and template starbursts

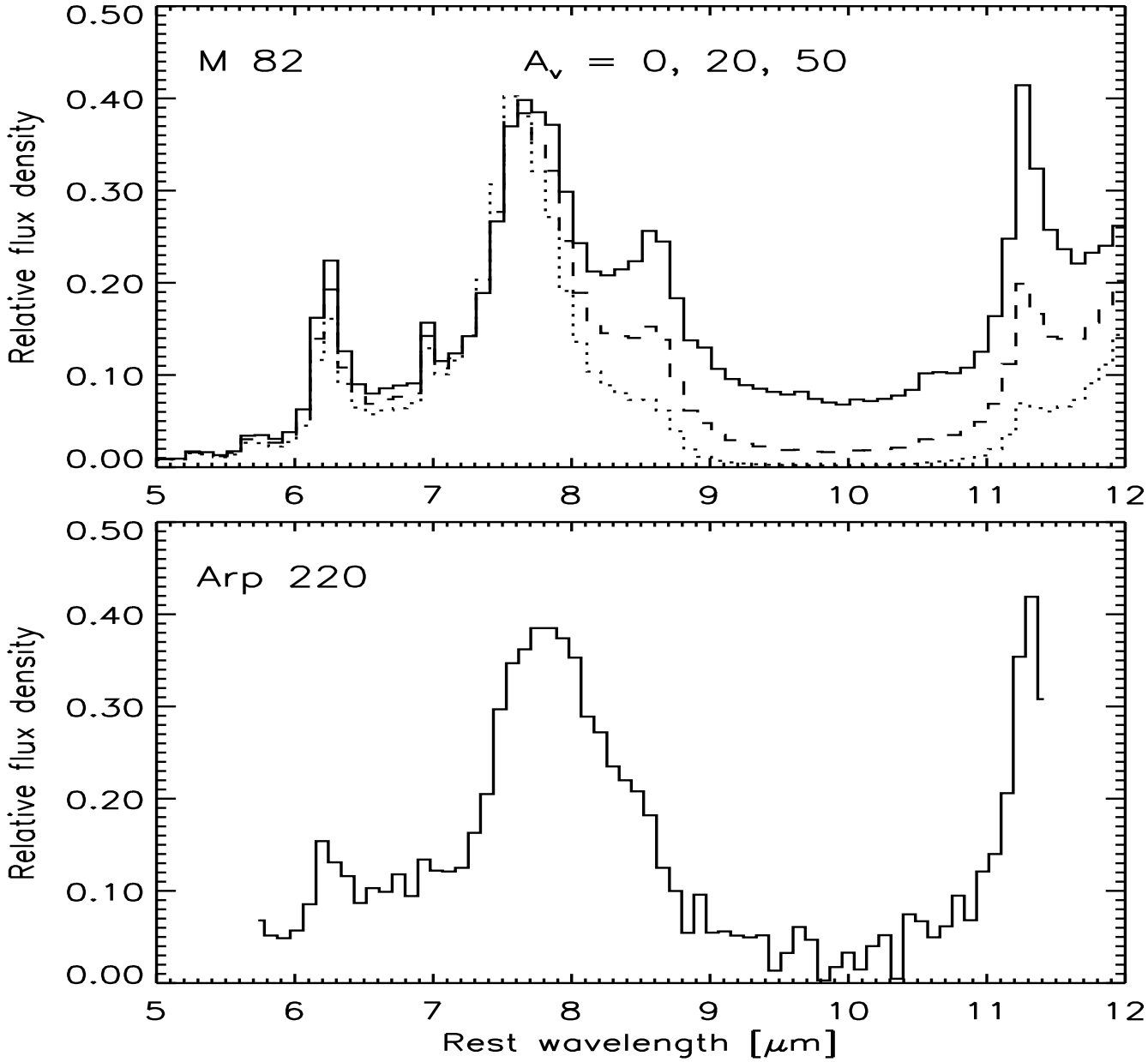

Fig. 6.— extincted M82 spectrum

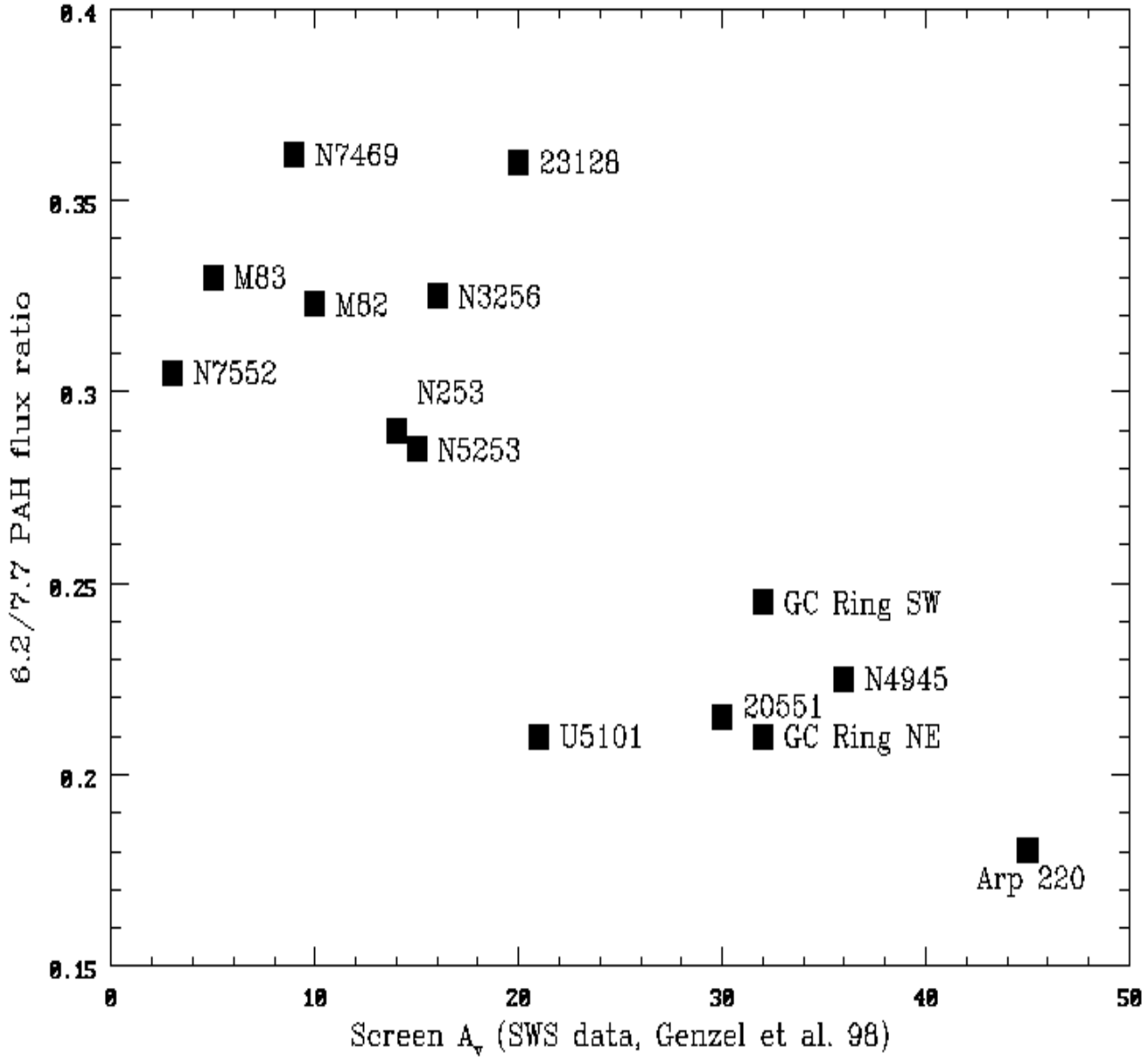

Fig. 7.— Effect of extinction on PAHs

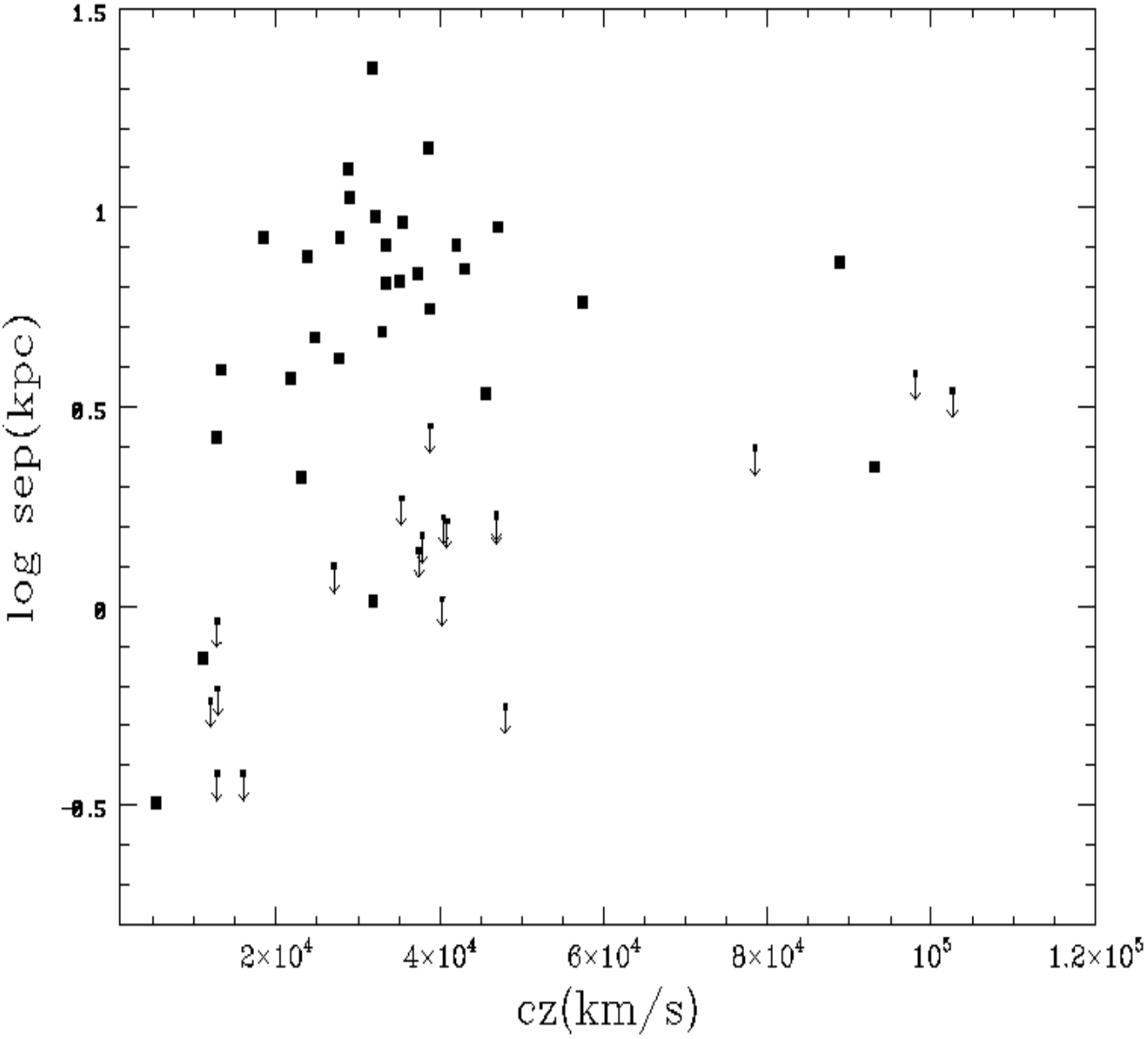

Fig. 8.— Projected nuclear separation as a function of redshift

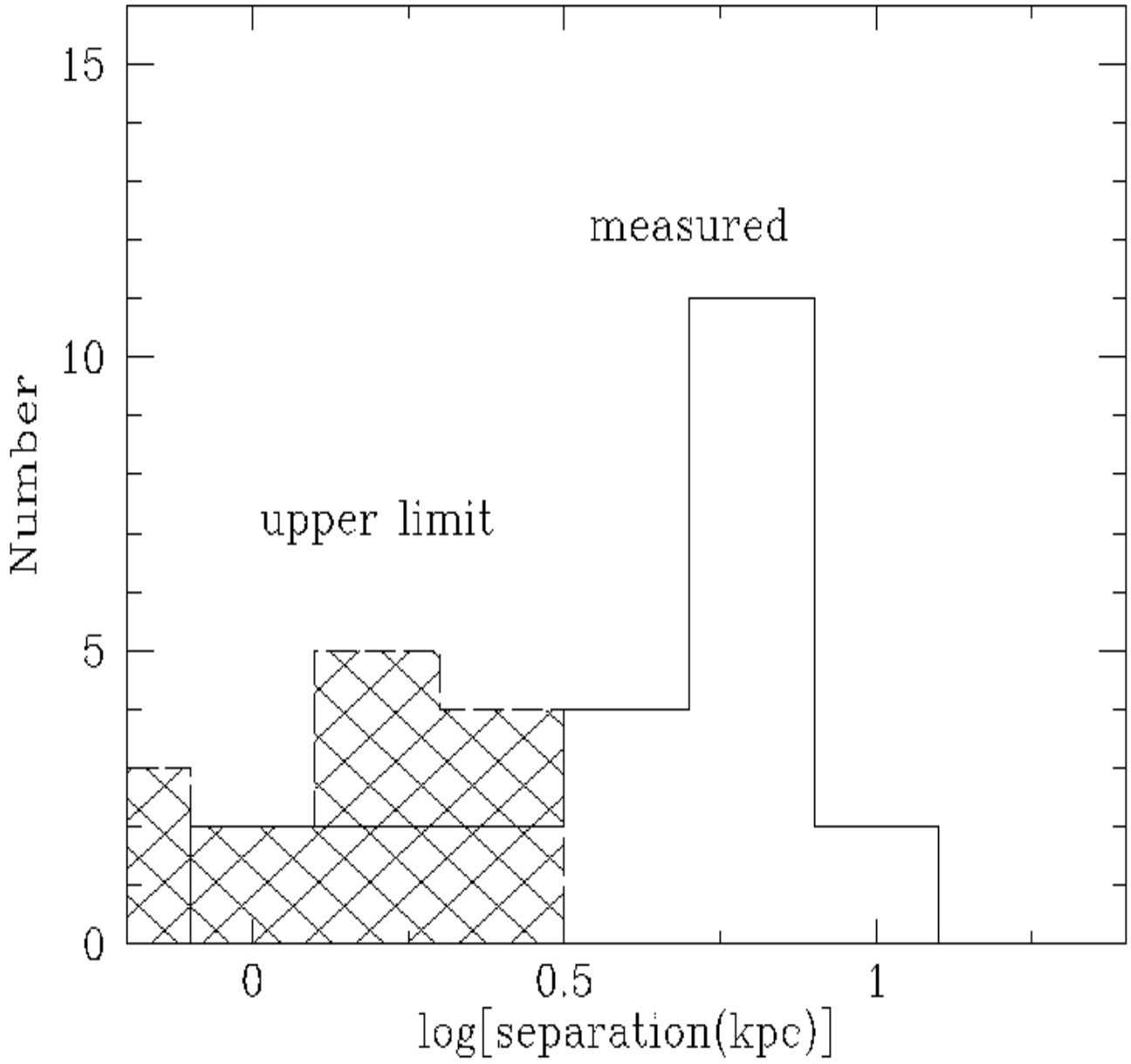

Fig. 9.— Histogram

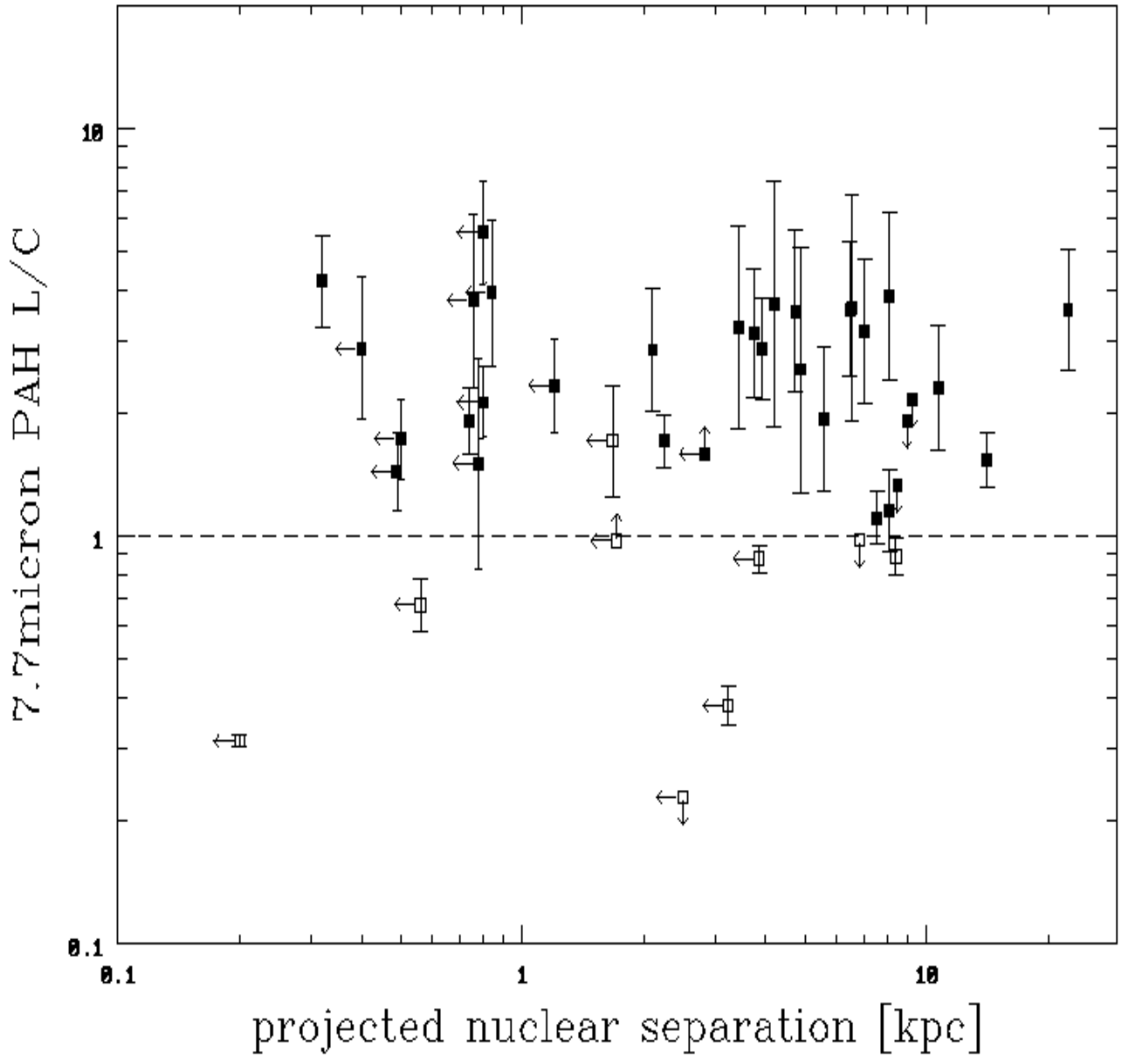

Fig. 10.— Separation plot

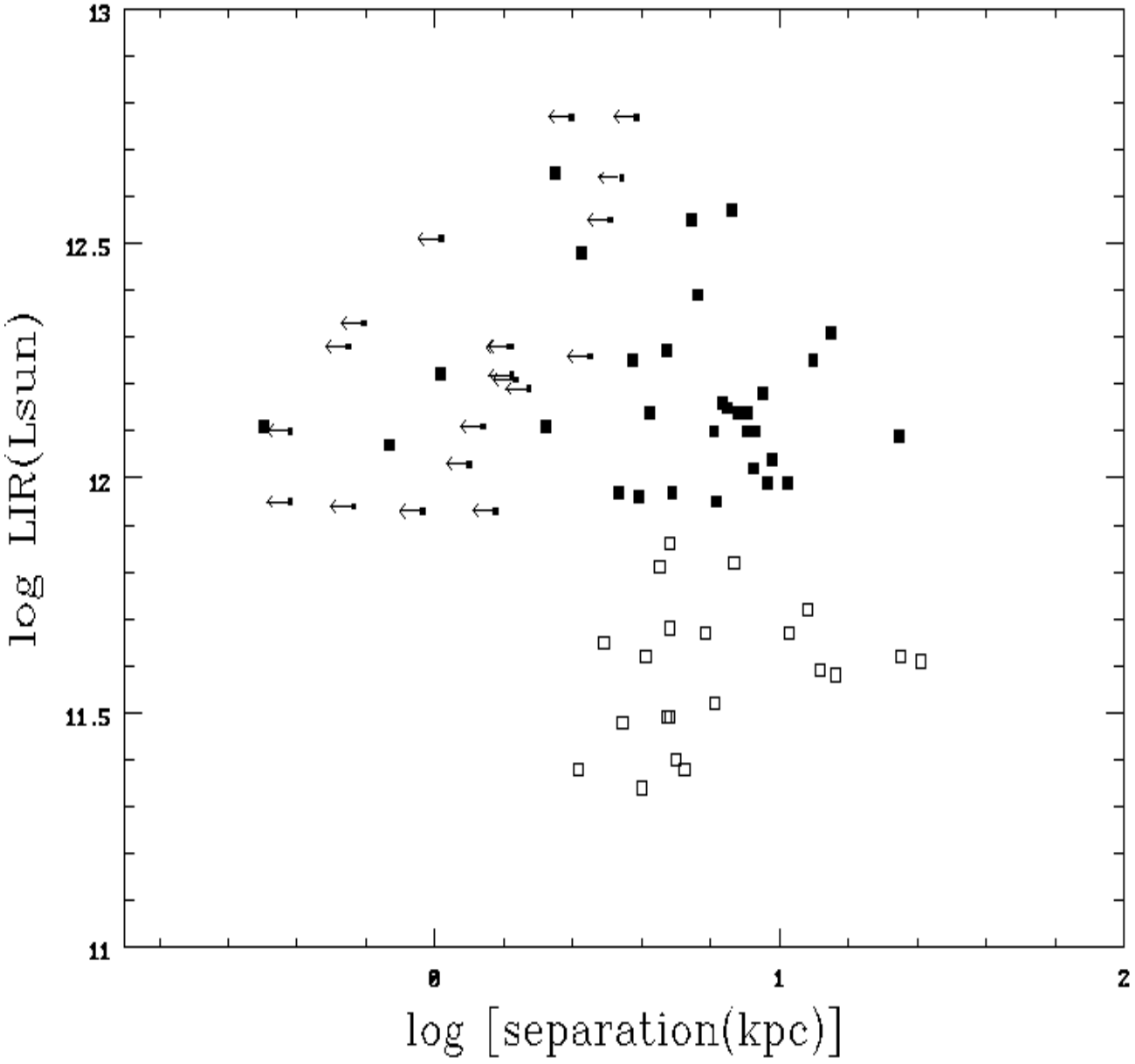

Fig. 11.— Luminosity-Separation plot

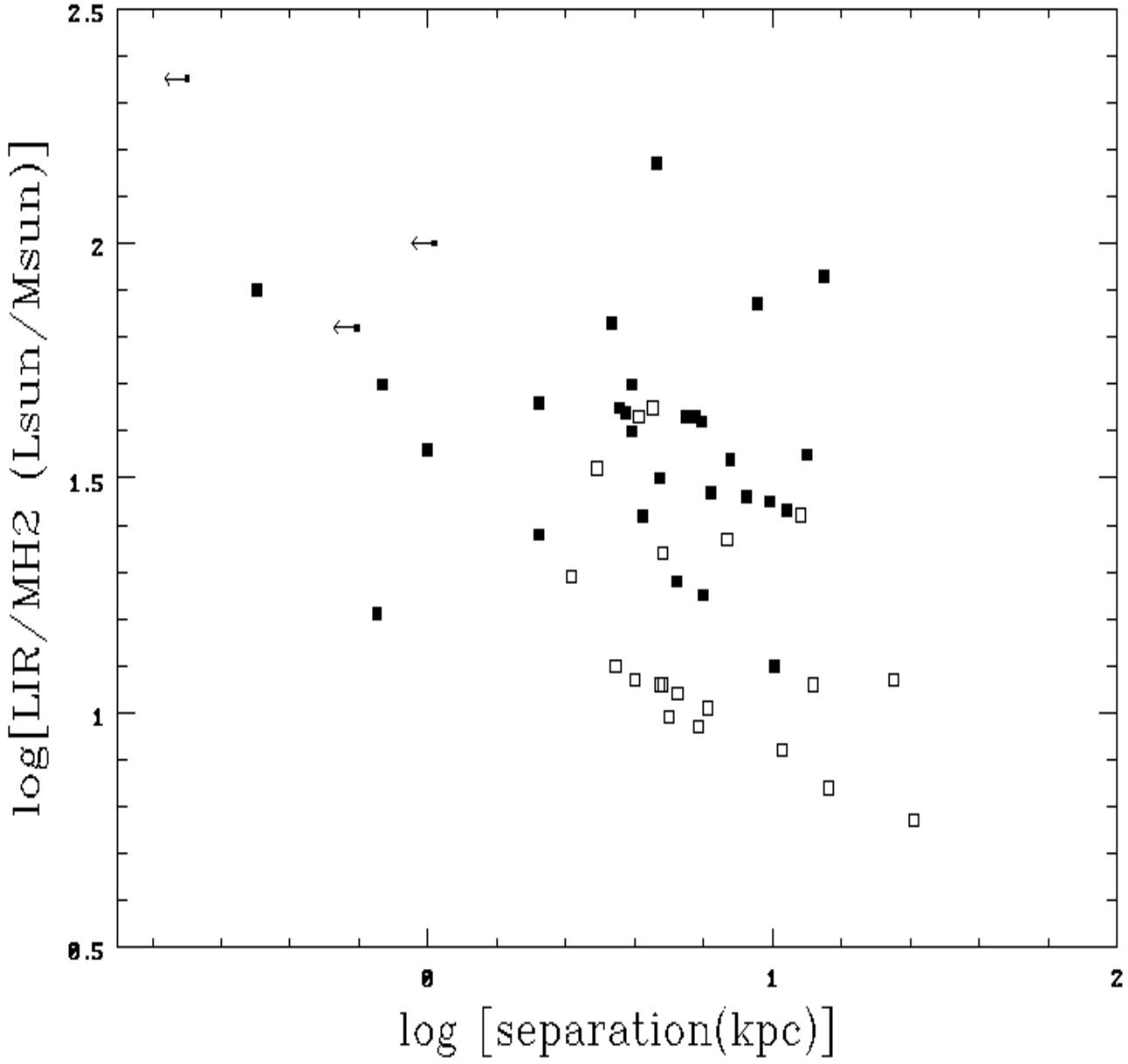

Fig. 12.— Star formation efficiency-Separation plot

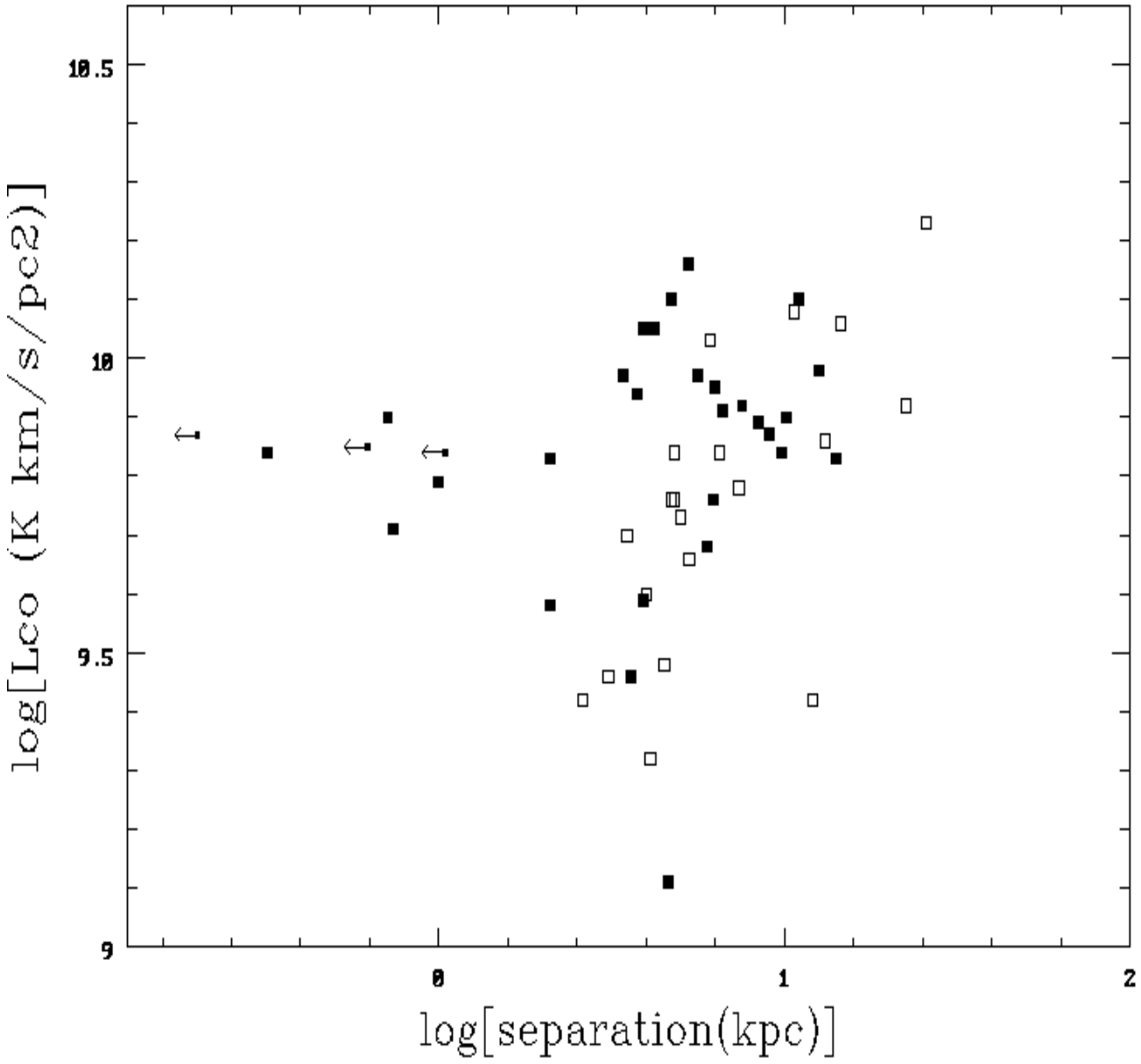

Fig. 13.— CO Luminosity-Separation plot